

## RESEARCH ARTICLE

10.1002/2016JC012629

## Key Points:

- Different optical behaviors among oceanic regions as observed from diffuse attenuation coefficients within the first optical depth
- High content of colored dissolved organic matter causes the deviation of most open ocean waters from existing bio-optical models
- Bio-optical anomalies as proxies for revealing the occurrence of specific events and related biogeochemical processes

## Correspondence to:

E. Organelli,  
emo@pml.ac.uk

## Citation:

Organelli, E., H. Claustre, A. Bricaud, M. Barbieux, J. Uitz, F. D'Ortenzio, and G. Dall'Olmo (2017), Bio-optical anomalies in the world's oceans: An investigation on the diffuse attenuation coefficients for downward irradiance derived from Biogeochemical Argo float measurements, *J. Geophys. Res. Oceans*, 122, 3543–3564, doi:10.1002/2016JC012629.

Received 14 DEC 2016

Accepted 17 MAR 2017

Accepted article online 23 MAR 2017

Published online 2 MAY 2017

## Bio-optical anomalies in the world's oceans: An investigation on the diffuse attenuation coefficients for downward irradiance derived from Biogeochemical Argo float measurements

Emanuele Organelli<sup>1,2</sup> , Hervé Claustre<sup>1</sup> , Annick Bricaud<sup>1</sup>, Marie Barbieux<sup>1</sup>, Julia Uitz<sup>1</sup>, Fabrizio D'Ortenzio<sup>1</sup> , and Giorgio Dall'Olmo<sup>2,3</sup> 

<sup>1</sup>Sorbonne Universités, UPMC Univ Paris 06, CNRS, UMR 7093, Laboratoire d'Océanographie de Villefranche (LOV), Villefranche-sur-mer, France, <sup>2</sup>Plymouth Marine Laboratory, Plymouth, UK, <sup>3</sup>National Centre for Earth Observation, Plymouth Marine Laboratory, Plymouth, UK

**Abstract** Identification of oceanic regions characterized by particular optical properties is extremely important for ocean color applications. The departure from globally established bio-optical models (i.e., anomaly) introduces uncertainties in the retrieval of biogeochemical quantities from satellite observations. Thanks to an array of 105 Biogeochemical Argo floats acquiring almost daily downward irradiance measurements at selected wavelengths in the UV and blue region of the spectrum, we reexamined the natural variability of the spectral diffuse attenuation coefficients,  $K_d(\lambda)$ , among the world's oceans and compared them to previously established bio-optical models. The analysis of 2847 measurements of  $K_d(\lambda)$  at 380 and 490 nm, within the first optical depth, provided a classification of the examined regions into three groups. The first one included the Black Sea, a water body characterized by a very high content of colored dissolved organic matter (CDOM). The second group was essentially composed by the subtropical gyres (Atlantic and Pacific Oceans), with optical properties consistent with previous models (i.e., no anomalies). High latitude (North Atlantic and Southern oceans) and temperate (Mediterranean Sea) seas formed the third group, in which optical properties departed from existing bio-optical models. Annual climatologies of the  $K_d(380)/K_d(490)$  ratio evidenced a persistent anomaly in the Mediterranean Sea, that we attributed to a higher-than-average CDOM contribution to total light absorption. In the North Atlantic subpolar gyre, anomalies were observed only in wintertime and were also attributed to high CDOM concentrations. In the Southern Ocean, the anomaly was likely related to high phytoplankton pigment packaging rather than to CDOM.

### 1. Introduction

In the 1970s and 1980s, the early years of development of modern optical oceanography, a few studies established empirical relationships between the concentration of chlorophyll *a*, a proxy of phytoplankton biomass, and the optical properties of the material dissolved or suspended in the seawater [Morel and Prieur, 1977; Gordon *et al.*, 1988; Morel, 1988]. The purpose was to investigate and analyze the variability of the optical properties of oceanic waters in order to extract biogeochemical quantities from the color of the ocean that could be potentially measured by the emerging satellite platforms [Morel and Prieur, 1977; Morel, 1988]. With this aim, Morel and Prieur [1977] introduced the distinction between Case 1 and Case 2 water types. Case 1 waters, i.e., most of the open ocean environments, were defined as those waters for which colored dissolved organic matter (CDOM) and nonalgal particles (NAP) are of autochthonous origin and covary with the concentration of chlorophyll *a* and other phytoplankton pigments regardless of their concentrations. On the contrary, Case 2 waters were defined as all the other aquatic environments for which the concentrations of algal pigments, dissolved and particulate materials varied independently [Morel and Prieur, 1977; Antoine *et al.*, 2014].

In the early 2000s, thanks to the emergence of more sophisticated analytical techniques (i.e., high performance liquid chromatography), the concentrations of chlorophyll *a* as well as of other phytoplanktonic pigments (xanthophylls and carotenoids) were determined with more accuracy [Vidussi *et al.*, 2001]. The bio-optical relationships were, therefore, reexamined [Morel and Maritorena, 2001; Bricaud *et al.*, 2004; Morel *et al.*, 2007b]. Morel and Maritorena [2001], in particular, reevaluated the relationships between optical

properties such as the spectral diffuse attenuation coefficients for downward irradiance,  $K_d(\lambda)$ , and chlorophyll *a* concentrations at the sea surface. The relationships established through these new databases became the most commonly used bio-optical models for open ocean waters and were applied at the global scale. The diffuse attenuation coefficients in the UV and visible domains were used to represent and explain the variations in the light absorption by CDOM (with NAP) and chlorophylls (together with other pigments), respectively, owing to their different spectral absorption properties [Bricaud *et al.*, 1981; Prieur and Sathyendranath, 1981; Bricaud *et al.*, 2004]. Hence,  $K_d(\lambda)$  values at given wavelengths emerged as optical proxies of biogeochemical quantities such as chlorophyll *a* and CDOM concentrations [Morel and Maritorena, 2001; Morel *et al.*, 2007a, 2007b].

The hypothesis that optical properties in some open ocean regions can diverge from the average of the world's oceans was early proposed [Mitchell and Holm-Hansen, 1991]. However, only recently, the natural variability around the mean statistical relationships has been analyzed for various optical properties [Morel *et al.*, 2007a; Szeto *et al.*, 2011; Huot and Antoine, 2016]. These studies evidenced that the optical behavior of several oceanic environments, in the UV and visible spectrum, is different. The main causes may be: (i) high CDOM content [Morel *et al.*, 2007a; Morel and Gentili, 2009a; Matsuoka *et al.*, 2011; Szeto *et al.*, 2011; Organelli *et al.*, 2014]; (ii) strong pigment packaging [Morel and Bricaud, 1981] of the phytoplankton community [Mitchell and Holm-Hansen, 1991; Mitchell, 1992; Szeto *et al.*, 2011] and/or presence/absence of accessory pigments reflecting a particular light history [Bricaud *et al.*, 2004, 2010]; (iii) occurrence of desert dusts [Claustre *et al.*, 2002; Claustre and Maritorena, 2003]. For example, when specifically addressing the mean statistical relationship between the diffuse attenuation coefficient of downward irradiance at 490 nm and chlorophyll *a* concentration, Morel *et al.* [2007a] found that two different environments such as the Mediterranean Sea and the South Pacific Ocean were represented by the average relationship of Morel and Maritorena [2001]. By contrast, the attenuation coefficients measured in the UV range were significantly higher in the Mediterranean Sea than the global average [Morel *et al.*, 2007a]. This departure from the model was attributed to the higher-than-average contribution of CDOM with respect to other oceanic regions, which was also later confirmed by other studies [Morel and Gentili, 2009b; Organelli *et al.*, 2014].

Identifying regions with such an anomalous optical behavior (hereafter called “bio-optical anomaly”) has an impact on ocean color applications and especially for the retrieval of bio-optical and biogeochemical products. When a bio-optical anomaly is observed, as in the Mediterranean Sea, the particular optical properties may introduce greater uncertainty into standard remote sensing inversion algorithms [D’Ortenzio *et al.*, 2002; Organelli *et al.*, 2016a]. Ocean-based regional algorithms could, instead, facilitate more acceptable retrievals [Bricaud *et al.*, 2002; Szeto *et al.*, 2011]. However, the undersampling that emerges from current in situ databases has so far limited the development of open ocean regional algorithms [Szeto *et al.*, 2011].

Over the last 5 years, a large array of autonomous Biogeochemical Argo floats (hereafter “BGC-Argo floats”) equipped with sensors for measuring inherent and apparent optical properties as well as biogeochemical variables [IOCCG, 2011; Biogeochemical-Argo Planning Group, 2016; Johnson and Claustre, 2016; Organelli *et al.*, 2016b] have been deployed in various open-ocean systems and trophic conditions. Contrarily to the traditional sampling from oceanographic vessels, BGC-Argo floats acquire data up to every 10 days, in remote areas (e.g., subtropical gyres, Arctic and Southern oceans), and even during periods with harsh seas that limit ship-based sampling. Thus, the number of vertical profiles for several bio-optical and biogeochemical variables has been dramatically increasing in few years. Therefore, the investigation of the bio-optical anomalies can be performed with unprecedented spatial and temporal resolutions, which is a prerequisite in view of characterizing nuances in mean bio-optical relationships at the regional scale.

This study examines the regional variability of relationships between CDOM (together with nonalgal particles) and phytoplankton light absorption properties with respect to previously established bio-optical models [Morel and Maritorena, 2001; Morel *et al.*, 2007b]. Diffuse attenuation coefficients of downward irradiance in the UV (i.e., 380 nm) and visible (i.e., 490 nm) over the world's oceans as derived from the existing BGC-Argo database [Organelli *et al.*, 2016c] are used as proxies of these two quantities. Analyses focused on the first optical depth (i.e., the layer of interest for satellite remote sensing) [Gordon and McCluney, 1975] allow identifying regions with bio-optical anomalies, for which ocean-based regional algorithms should be consolidated to improve the retrieval of biogeochemical quantities from remote sensing ocean color observations. The temporal variability around the mean statistical relationships is explored—for the first time—for a comprehensive set of oceanic regions representative of diverse trophic and bio-optical conditions.

Finally, possible factors causing the bio-optical anomalies are discussed with the help of concurrent measurements of other variables such as chlorophyll *a* concentration, fluorescent dissolved organic matter, and the particle light backscattering coefficient.

## 2. Materials and Methods

### 2.1. The BGC-Argo Database

An array of 105 "PROVOR-CTS4" profiling floats was deployed in several areas of the world's oceans in the frame of several research programs (Figure 1; see acknowledgements). Each float acquired vertical profiles of optical and bio-optical variables (downward irradiance  $E_d(\lambda)$ , Photosynthetically Available Radiation PAR, chlorophyll *a* fluorescence Chl, dissolved organic matter fluorescence FDOM, and particle light backscattering coefficient  $b_{bp}(\lambda)$ ) in addition to temperature (T) and salinity (S). Upward casts were programmed every 1, 2, 3, 5, or 10 days depending on the mission and scientific objectives. Each cast started from the 1000 m parking depth at sufficient time for surfacing around local noon. Data acquisition was nominally 10 m resolution between 250 and 1000 m of depth, 1 m resolution between 10 and 250 m, and increased at 0.20 m resolution between 10 m and the surface [Organelli et al., 2016b].

A total of 9837 BGC-Argo stations, each one corresponding to an upward cast collected between October 2012 and January 2016, were used in this study (Figure 1). All stations were checked for possible corruption by biofouling (a profiling float spends most of its time in dark and cold 1000 m waters, which naturally prevents or delays biofilm formation) or any instrumental drift. The stations were then grouped in 25 geographic areas (Table 1) encompassing a wide range of oceanic conditions, from subpolar to tropical and from eutrophic systems to oligotrophic mid-ocean gyres. In the following sections, data analysis and quality-control protocols are briefly reported for each measured and derived parameter. Finally, the use of the quality-controlled variables to identify and explain the optical behavior of the various oceanic areas is also presented.

### 2.2. Radiometry and Diffuse Attenuation Coefficients for Downward Irradiance

The profiling floats were equipped with a multispectral ocean color radiometer (OCR-504, SATLANTIC Inc.) providing 0–250 m profiles of  $E_d(\lambda)$  at three wavelengths (i.e., 380, 412, and 490 nm) and PAR integrated

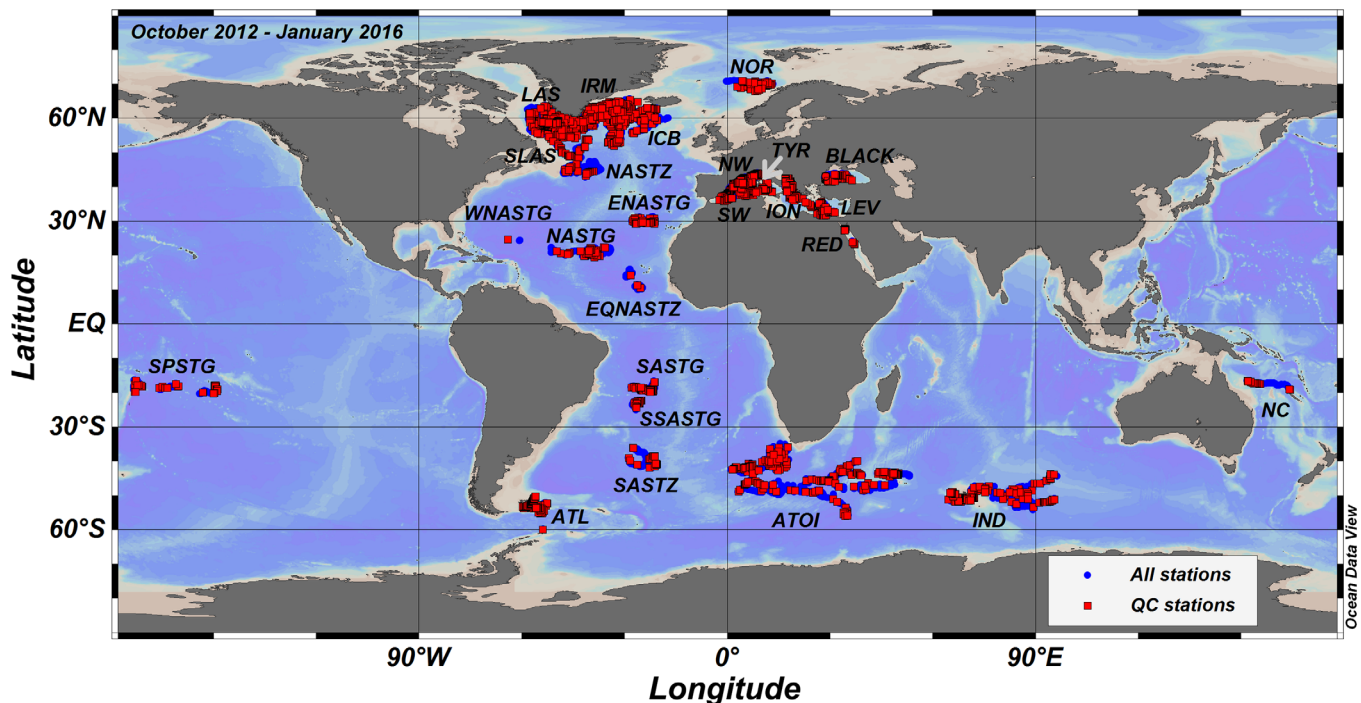


**Figure 1.** The 9837 stations sampled by 105 Biogeochemical Argo floats between October 2012 and January 2016. Squares indicate the 2847 quality-controlled (QC) stations with simultaneous  $K_{bio}(380)$  and  $K_{bio}(490)$  coefficients used for identification of bio-optical anomalies. Abbreviations for the 25 geographic areas are displayed (see Table 1 for full description). The map is drawn by the Ocean Data View software [R. Schlitzer, Ocean Data View, <http://odv.awi.de>].

**Table 1.** Basin, Abbreviation, and Number of Floats for 25 Geographic Areas Included in the Biogeochemical Argo Database<sup>a</sup>

Region	Basin	Abbreviation	Float No.
Arctic Sea	Norwegian Sea	NOR	1
Black Sea	Black Sea	BLACK	4
Western Mediterranean Sea	Northwestern Southwestern	NW SW	9 6
Eastern Mediterranean Sea	Tyrrhenian Sea Ionian Sea	TYR ION	6 8
North Atlantic subpolar gyre	Levantine Sea	LEV	7
North Atlantic subtropical gyre	Labrador Sea	LAS	15
	Irminger Sea	IRM	11
	Iceland Basin	ICB	8
	South Labrador Sea	SLAS	2
	Transition zone	NASTZ	1
North Atlantic subtropical gyre	Subtropical gyre	NASTG	4
	Eastern subtropical gyre	ENASTG	2
	Western subtropical gyre	WNASTG	2
Red Sea	Transition zone	EQNASTZ	2
South Atlantic Ocean	Red Sea	RED	2
	Subtropical gyre	SASTG	3
	South subtropical gyre	SSASTG	1
South Pacific Ocean	Transition Zone	SASTZ	2
	Subtropical gyre	SPSTG	3
	New Caledonia	NC	2
Southern Ocean	Atlantic sector	ATL	3
	Atlantic to Indian sector	ATOI	10
	Indian sector	IND	6

<sup>a</sup>Note that the total number of floats is >105 because some floats moved across two or more basins during their lifetime.

over 400–700 nm. Electronic counts were converted into radiometric quantities (in units of:  $\mu\text{W cm}^{-2} \text{nm}^{-1}$  for  $E_d(\lambda)$ ;  $\mu\text{mol quanta m}^{-2} \text{s}^{-1}$  for PAR) according to SATLANTIC [2013] and using specific calibration coefficients for each channel of each sensor.

Radiometric profiles were quality-controlled following protocols and procedures specifically developed for autonomous measurements by *Organelli et al.* [2016b]. Current dark, atmospheric clouds, and wave focusing [*Zaneveld et al.*, 2001] occurrences were flagged and removed from each profile. Measurements performed during very unstable sky and sea conditions were also identified and disregarded. No dark offset adjustment and correction for sensor’s water temperature dependence [*Mueller et al.*, 2003] were applied, as they have a negligible impact on surface radiometric quantities of interest for this study [*Organelli et al.*, 2016b].

For each quality-controlled profile,  $E_d(0^-)$  and PAR just below the sea surface were extrapolated within the first optical depth ( $Z_{pd}$ ) using a second-degree polynomial function [*Organelli et al.*, 2016b]. Following *Morel* [1988], the first optical depth was computed as  $Z_{eu}/4.6$  where the euphotic depth,  $Z_{eu}$ , is the depth at which PAR is reduced to 1% of its value just below the sea surface. A total of 5767 stations with quality-controlled  $Z_{eu}$  and  $Z_{pd}$  values were retained. Then, the corresponding  $E_d(\lambda)$  profiles were binned every 1 m and the diffuse attenuation coefficients ( $K_d(\lambda)$ ; in units of  $\text{m}^{-1}$ ) were obtained from a linear fit between the natural logarithm of  $E_d(\lambda)$  and depths within  $Z_{pd}$  [*Mueller et al.*, 2003]. Check for  $E_d(\lambda)$  outlier values was done before  $K_d(\lambda)$  computation.  $K_d(\lambda)$  values resulting from linear fits based on less than 3 points or with a determination coefficient ( $r^2$ ) lower than 0.90 were excluded from the analysis. Hence, a total of 4162, 3956, and 3557 values for  $K_d(380)$ ,  $K_d(412)$ , and  $K_d(490)$  coefficients, respectively, were retained. Standard errors of  $K_d(\lambda)$  values were also obtained from linear fits. They varied between 0.0002–0.088, 0–0.098, and 0–0.083  $\text{m}^{-1}$  for  $K_d(380)$ ,  $K_d(412)$ , and  $K_d(490)$  coefficients, respectively.

### 2.3. Chlorophyll a, Fluorescent Dissolved Organic Matter, and Particle Light Backscattering

A WETLabs ECO sensor installed on each float provided simultaneous 0–1000 m profiles of chlorophyll *a* (excitation/emission: 470/695 nm) and dissolved organic matter (excitation/emission: 370/460 nm) fluorescence, and of the angular scattering coefficient ( $\beta(\theta, \lambda)$ ) at 700 nm measured at an angle of 124°. For each parameter, raw counts were converted in desired quantities and units using the calibration coefficients provided by the manufacturer.

The quality control of chlorophyll *a*, Chl (in units of  $\text{mg m}^{-3}$ ), was performed following the procedures described in *Schmechtig et al.* [2014]. Corrections aimed at adjusting the profile for no-zero dark values, identifying the occurrences of negative spikes, and verifying the range of measured values according to technical specifications provided by the manufacturer [*WETLabs*, 2016]. A correction for the nonphotochemical quenching [*Kiefer*, 1973] was also performed following *Xing et al.* [2012]. In specific areas (e.g., Black Sea), chlorophyll *a* concentration showed a tendency to increase at depth where it was supposed to be zero. This behavior was associated to the influence of fluorescent dissolved organic matter [*Proctor and Roesler*, 2010] and corrected according to the procedures established by *Xing et al.* [2017]. Finally, following the recommendations by *Roesler et al.* [2017] on the evidence of a factory calibration bias in the estimated

chlorophyll *a* concentrations from WETLab ECO series chlorophyll fluorometers, each quality-controlled chlorophyll *a* value was divided by 2 to improve accuracy of measurements for applications at the global scale. The correction factor was deduced from a global comparison of fluorescence with paired HPLC Chl observations, and confirmed by HPLC-calibrated optical proxies of Chl such as the light absorption line height [Roesler and Barnard, 2013].

The quality control of fluorescent dissolved organic matter, FDOM (in units of ppb), was executed according to the following procedures. First, the range of measured values was verified following the technical specifications provided by the manufacturer [WETLabs, 2016]. Then, spikes were identified and removed. The BGC-Argo floats included in this database spent their life without moving substantially among different deep water masses. This, together with the assumption that the deep concentration of dissolved organic material is conservative in a given water body [Nelson et al., 2007], allows profiles collected by a given float to be scaled with confidence to the FDOM value measured by the first cast of the time series between 950 and 1000 m. Finally, remaining spikes were removed by applying a median filter (5 point window) and an average filter (7 point window) was then used to smooth the profile.

Following the procedures described in Schmechtig et al. [2016], the particle backscattering coefficient at 700 nm ( $b_{bp}(700)$ ; in units of  $m^{-1}$ ) was obtained by removing the contribution of pure seawater [Zhang et al., 2009] from  $\beta(124^\circ, 700)$  and then applying a conversion to total particle backscattering according to procedures and constants in Boss and Pegau [2001] and Sullivan et al. [2013]. Vertical profiles of  $b_{bp}(700)$  were then quality controlled by verifying the range of measured values according to the technical specifications provided by the manufacturer [WETLabs, 2016] and removing negative spikes following Briggs et al. [2011]. Other spikes were additionally removed by applying a median filter (5 point window).

Finally, all quality-controlled profiles of Chl, FDOM, and  $b_{bp}(700)$  were binned every 1 m and the average (with standard deviation) within  $Z_{pd}$  was computed.

#### 2.4. Identification of Bio-Optical Anomalies

The investigation on bio-optical anomalies involved analysis of 2847 simultaneous vertical profiles of diffuse attenuation coefficients for downward irradiance at 380 and 490 nm ( $K_d(380)$  and  $K_d(490)$ ) within the first optical depth. Because of their physical nature (i.e., ratio of  $E_d(\lambda)$  values within the same profile),  $K_d(\lambda)$  values are quasi-insensitive to instrument calibration issues and/or sensor drifts, thus revealing to be robust parameters for the investigation of ocean's optical behavior over time.  $K_d(380)$  and  $K_d(490)$  coefficients were used to estimate the variations in the light absorption by CDOM and NAP, and by phytoplankton, respectively. The  $K_d(\lambda)$  coefficients can be expressed as [Gordon, 1989]:

$$K_d = 1.04(\mu_d)^{-1}(a + b_b) \quad (1)$$

where  $a$  and  $b_b$  are the total light absorption and backscattering coefficients, respectively, and  $b_b$  is typically a few percent of the total absorption coefficient, except in extremely clear waters where it may occasionally reach 25% in the blue-violet region of the light spectrum [Morel et al., 2007a]. In equation (1),  $\mu_d$  is the average cosine for downward irradiance  $E_d$  which depends on solar elevation, wavelength, and chlorophyll *a* concentration [Morel and Loisel, 1998]. Values of  $\mu_d(\lambda)$  were calculated using the mean chlorophyll *a* concentration within  $Z_{pd}$  of each profile, a solar zenith angle between 0 and 75°, and an optical thickness at 550 nm of 0.05 due to the aerosol [Morel and Loisel, 1998]. The  $\mu_d(\lambda)$  values varied in the ranges 0.692–0.927 and 0.679–0.948 for 380 and 490 nm, respectively, in agreement with Morel et al. [2007a].

Following Morel [1988], the constant contribution to attenuation of pure sea water ( $K_w(\lambda)$ ) [Morel and Maritorena, 2001] was removed from  $K_d(\lambda)$  and the quantity  $K_{bio}(\lambda)$  was obtained as:

$$K_{bio}(\lambda) = K_d(\lambda) - K_w(\lambda) \quad (2)$$

Only  $K_{bio}(\lambda) > 0.002 m^{-1}$  (i.e.,  $K_d(\lambda)$  higher than 10%  $K_w(\lambda)$ ) were found to be reliable and used for the following analyses. A linear regression analysis was performed on the log-transforms of each  $K_{bio}(\lambda)$  pair for the whole data set. Regression coefficients were then compared to the previously established bio-optical models by Morel and Maritorena [2001] and Morel et al. [2007b] representative of the “mean statistical relationships.” To identify regional bio-optical anomalies, a Student's *t*-test was first applied to check if the average distance of points within a given region departed significantly ( $\alpha = 0.05$ ) from the Morel et al. [2007b]

relationship. Second, linear regressions on the log-transforms of  $K_{\text{bio}}(\lambda)$  within each region were calculated after removal of outliers on the residuals according to the Jackknife method [Tukey, 1958]. For significant regression fits ( $\alpha = 0.01$ ), a test of parallelism ( $\alpha = 0.01$ ) was then used to verify the significance of the differences of regression coefficients with respect to the Morel *et al.* [2007b] model. Finally, the temporal variability of each region around the mean statistical relationships was explored comparing the monthly climatology of the ratio between  $K_{\text{bio}}(380)$  and  $K_{\text{bio}}(490)$ , calculated as the average of all ratios within  $Z_{\text{pd}}$  in a given region for a given month, to the average ratio obtained from Morel *et al.* [2007b] relationships (and computed for chlorophyll *a* ranges measured by BGC-Argo floats).

### 2.5. Understanding the Sources of the Anomalies

Monthly climatologies of chlorophyll *a*, FDOM and their ratio were used to interpret the bio-optical behavior observed from the analysis of  $K_{\text{bio}}(\lambda)$  coefficients and explain the variability of  $K_{\text{bio}}(380)/K_{\text{bio}}(490)$  ratios. Cross-correlation analysis ( $\alpha = 0.05$ ) was also performed between the two ratios in order to measure the time lag. To identify any possible dependence of  $K_{\text{bio}}(\lambda)$  values on specific optical properties of the phytoplankton community [e.g., “packaging effect,” Morel and Bricaud, 1981], the relationships between  $K_{\text{bio}}(490)$  and chlorophyll *a* concentration were examined and compared to the bio-optical model by Morel *et al.* [2007b]. Finally, relationships between  $K_{\text{bio}}(490)$  and  $b_{\text{bp}}(700)$  were used to address to what extent and in which region the particle light backscattering might contribute to enhance  $K_{\text{bio}}(\lambda)$  values as a consequence of, e.g., the presence of more abundant scattering particles.

## 3. Results and Discussion

### 3.1. Global Spectral Variability of Diffuse Attenuation Coefficients and Deviations From Mean Statistical Relationships

The spectral variations of the nonwater diffuse attenuation coefficients ( $K_{\text{bio}}(\lambda)$ ) are displayed in Figure 2. From the linear regression on log-transformed data, the relationship of  $K_{\text{bio}}(380)$  as a function of  $K_{\text{bio}}(490)$  can be expressed as a power law (Figure 2a):

$$K_{\text{bio}}(380) = 0.944 (\pm 0.010) * K_{\text{bio}}(490)^{0.754 (\pm 0.007)} \quad (n=2847, r^2=0.81) \quad (3)$$

with standard errors of linear regression coefficients on log-transformed quantities in parentheses.

This relationship can be compared to that established by Morel and Maritorena [2001]:

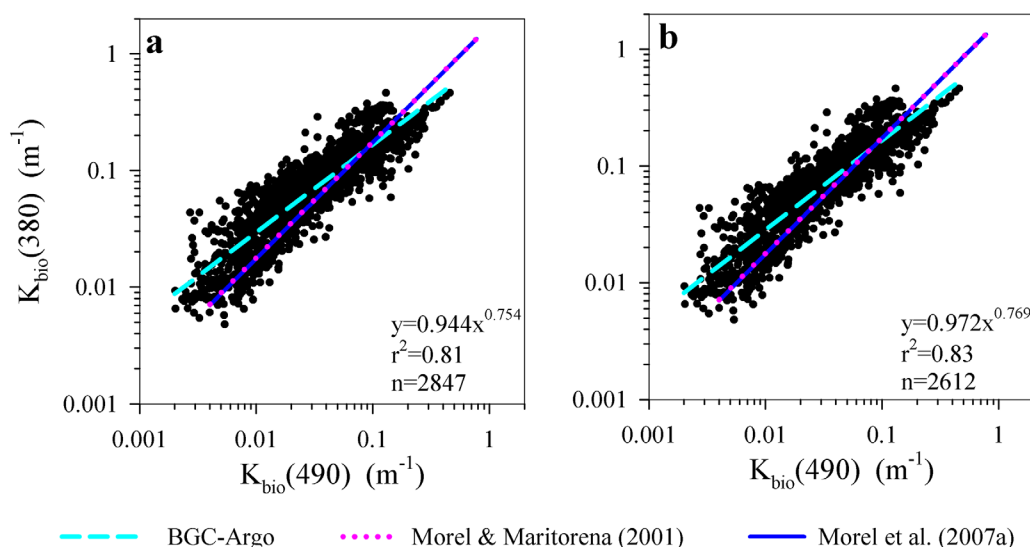


**Figure 2.** Log-log plot of  $K_{\text{bio}}(380)$  as a function of  $K_{\text{bio}}(490)$ : (a) all measurements collected by BGC-Argo floats within the first optical depth; (b) measurements collected by BGC-Argo floats within the first optical depth and a solar zenith angle between 0 and 75°. In each plot, the regression line for BGC-Argo measurements is displayed as a dashed line and statistics are shown. Previous regression lines from Morel and Maritorena [2001] and Morel *et al.* [2007b] are shown for comparison and are limited to the range of  $K_{\text{bio}}(490)$  values found in those studies.

$$K_{\text{bio}}(380) = 1.723 * K_{\text{bio}}(490)^{0.993}, \quad (4)$$

and the one calculated from the database by *Morel et al.* [2007b] using  $K_{\text{bio}}(\lambda) > 0.002 \text{ m}^{-1}$  (standard errors of linear regression coefficients on log-transformed data in parentheses):

$$K_{\text{bio}}(380) = 1.721(\pm 0.046) * K_{\text{bio}}(490)^{0.996(\pm 0.028)} \quad (n=220, r^2=0.85) \quad (5)$$

Deviations of the BGC-Argo database from the mean statistical relationships appear (Figure 2a). BGC-Argo derived  $K_{\text{bio}}(380)$  and  $K_{\text{bio}}(490)$  coefficients are consistent with the range of ship-based observations in *Morel and Maritorena* [2001] and *Morel et al.* [2007b] studies, but for  $K_{\text{bio}}(490)$  values  $< 0.004 \text{ m}^{-1}$  (i.e.,  $K_d(490) < 0.02 \text{ m}^{-1}$ ). The range of BGC-Argo  $K_d(490)$  coefficients, and thus of  $K_{\text{bio}}(490)$  values, is also in good agreement with ship-based measurements archived within other global compilations [*Valente et al.*, 2016]. However,  $K_{\text{bio}}(380)$  values are generally higher than those previously observed for a given  $K_{\text{bio}}(490)$ , with the difference increasing toward the lowest  $K_{\text{bio}}(490)$  coefficients (Figure 2a). Contrary to what was found by *Morel and Maritorena* [2001] and *Morel et al.* [2007b] (equations (4) and (5)), the exponent in equation (3) also reveals that the relationship between the attenuation coefficients at the two selected wavelengths is nonlinear.

The main cause of the observed deviations is due to the different geographic distribution of the databases. The study by *Morel and Maritorena* [2001] is mainly based on data collected in ultra to moderately oligotrophic environments (e.g., subtropical gyres) and only few samples were collected in mesotrophic to eutrophic waters. The *Morel et al.* [2007b] relationship is an updated version of the *Morel and Maritorena* [2001]'s model with the addition of data collected in the Eastern South Pacific Ocean [BIOSOPE area; *Claustre et al.*, 2008], in the Mediterranean Sea during summer-early autumn and a few from the Benguela Current [*Morel et al.*, 2007b]. Therefore, previous models are very likely biased toward oligotrophic environments. The 25 regions of the BGC-Argo database used in this study cover a large diversity of trophic situations, encompassing waters from the oligotrophic subtropical gyres to the highly productive areas of the North Atlantic subpolar gyre, Southern Ocean and North Western Mediterranean Sea, and also include the transition zones between one regime and another.

In addition, the *Morel and Maritorena* [2001] and *Morel et al.* [2007b] data sets are compiled with data from oceanographic cruises generally carried out during periods and seasons characterized by suitable meteorological conditions for sampling. This ultimately introduces also a temporal bias. The BGC-Argo floats are designed to routinely acquire profiles anytime, regardless of sea conditions. As a consequence, the relationship in equation (3) is based on data acquired in wintertime in areas such as the North Atlantic subpolar gyre, the subtropical gyres and the Southern Ocean, data that are not included in previous relationships.

The relationship in equation (3) includes  $K_{\text{bio}}(\lambda)$  coefficients acquired at high latitudes where the solar elevation could be too low and unsuitable for measuring downward irradiance even at local noon [*Mueller et al.*, 2003]. In Figure 2b, only  $K_{\text{bio}}(\lambda)$  values derived from radiometric measurements acquired with 0–75° sun zenith angles are shown and the relationship can be expressed as (standard errors of linear regression coefficients on log-transformed data in parentheses):

$$K_{\text{bio}}(380) = 0.972(\pm 0.010) * K_{\text{bio}}(490)^{0.769(\pm 0.007)} \quad (n=2612, r^2=0.83) \quad (6)$$

Removed samples are mainly from the Norwegian Sea, North Atlantic subpolar gyre, and Southern Ocean in late autumn and wintertime. The regression and determination ( $r^2$ ) coefficients slightly increase compared to equation (3) but deviations from the mean statistical relationships still appear (Figure 2b). Hence, these samples with low solar elevation do not significantly affect the global trend, and thus they are kept for the following analyses.

### 3.2. Regional Variability of Diffuse Attenuation Coefficients and Deviations From Mean Statistical Relationships

The Black Sea shows the highest average  $K_{\text{bio}}(380)$  and  $K_{\text{bio}}(490)$  coefficients within the database (Table 2; Figure 3). Among high latitude open ocean waters, the North Atlantic subpolar gyre shows the highest  $K_{\text{bio}}(380)$  and  $K_{\text{bio}}(490)$  coefficients.  $K_{\text{bio}}(380)$  values range from  $0.115 \pm 0.045 \text{ m}^{-1}$  to  $0.144 \pm 0.060 \text{ m}^{-1}$ , while  $K_{\text{bio}}(490)$  coefficients vary between  $0.065 \pm 0.048 \text{ m}^{-1}$  and  $0.082 \pm 0.066 \text{ m}^{-1}$  in the Irminger and Labrador Seas, respectively (Table 2; Figure 3). The Southern Ocean has, instead, lower average  $K_{\text{bio}}(\lambda)$

**Table 2.** Minimum, Maximum, Mean ( $\pm$  Standard Deviation) and Number (N) of  $K_{bio}(380)$  and  $K_{bio}(490)$  Coefficients for the 25 Geographic Areas Included in the Biogeochemical Argo Database<sup>a</sup>

Region	Basin	N	$K_{bio}(380)$ ( $m^{-1}$ )			$K_{bio}(490)$ ( $m^{-1}$ )		
			Min	Max	Mean $\pm$ SD (CV)	Min	Max	Mean $\pm$ SD (CV)
Arctic Sea	Norwegian Sea	42	0.053	0.230	0.125 $\pm$ 0.046 (37%)	0.010	0.156	0.053 $\pm$ 0.033 (62%)
Black Sea	Black Sea	81	0.162	0.460	0.298 $\pm$ 0.048 (16%)	0.026	0.149	0.093 $\pm$ 0.026 (28%)
Western Mediterranean Sea	Northwestern	228	0.031	0.280	0.110 $\pm$ 0.046 (42%)	0.005	0.267	0.064 $\pm$ 0.048 (75%)
	Southwestern	171	0.027	0.204	0.091 $\pm$ 0.032 (35%)	0.004	0.146	0.046 $\pm$ 0.025 (54%)
Eastern Mediterranean Sea	Tyrrhenian Sea	94	0.019	0.134	0.079 $\pm$ 0.028 (35%)	0.003	0.093	0.033 $\pm$ 0.019 (58%)
	Ionian Sea	245	0.013	0.181	0.065 $\pm$ 0.026 (40%)	0.003	0.073	0.024 $\pm$ 0.013 (54%)
North Atlantic subpolar gyre	Levantine Sea	92	0.010	0.117	0.037 $\pm$ 0.021 (57%)	0.003	0.081	0.015 $\pm$ 0.014 (93%)
	Labrador Sea	498	0.051	0.461	0.144 $\pm$ 0.060 (42%)	0.009	0.460	0.082 $\pm$ 0.066 (80%)
North Atlantic subtropical gyre	Irminger Sea	213	0.054	0.350	0.115 $\pm$ 0.045 (39%)	0.005	0.353	0.065 $\pm$ 0.048 (74%)
	Iceland Basin	244	0.057	0.300	0.125 $\pm$ 0.044 (35%)	0.011	0.255	0.073 $\pm$ 0.044 (60%)
	South Labrador Sea	15	0.073	0.124	0.100 $\pm$ 0.015 (15%)	0.019	0.069	0.039 $\pm$ 0.016 (41%)
	Transition zone	25	0.081	0.203	0.142 $\pm$ 0.039 (27%)	0.030	0.124	0.070 $\pm$ 0.024 (34%)
North Atlantic subtropical gyre	Subtropical gyre	67	0.008	0.041	0.019 $\pm$ 0.006 (32%)	0.004	0.030	0.011 $\pm$ 0.005 (45%)
	Eastern subtropical gyre	37	0.009	0.086	0.040 $\pm$ 0.018 (45%)	0.003	0.064	0.020 $\pm$ 0.012 (60%)
	Western subtropical gyre	1	0.024			0.011		
	Transition zone	3	0.030	0.040	0.035 $\pm$ 0.005 (14%)	0.017	0.021	0.019 $\pm$ 0.002 (11%)
Red Sea	Red Sea	22	0.013	0.061	0.043 $\pm$ 0.017 (40%)	0.003	0.047	0.020 $\pm$ 0.011 (55%)
South Atlantic Ocean	Subtropical gyre	91	0.006	0.033	0.014 $\pm$ 0.006 (43%)	0.002	0.031	0.007 $\pm$ 0.005 (71%)
	South subtropical gyre	23	0.008	0.028	0.013 $\pm$ 0.005 (38%)	0.002	0.020	0.007 $\pm$ 0.004 (57%)
South Pacific Ocean	Transition Zone	31	0.044	0.108	0.073 $\pm$ 0.017 (23%)	0.014	0.074	0.044 $\pm$ 0.017 (39%)
	Subtropical gyre	45	0.005	0.032	0.013 $\pm$ 0.006 (46%)	0.003	0.022	0.009 $\pm$ 0.004 (44%)
Southern Ocean	New Caledonia	23	0.011	0.049	0.025 $\pm$ 0.009 (36%)	0.004	0.029	0.014 $\pm$ 0.008 (57%)
	Atlantic sector	129	0.023	0.317	0.069 $\pm$ 0.054 (78%)	0.003	0.271	0.046 $\pm$ 0.055 (120%)
Southern Ocean	Atlantic to Indian sector	228	0.027	0.136	0.062 $\pm$ 0.019 (31%)	0.007	0.140	0.038 $\pm$ 0.020 (53%)
	Indian sector	199	0.026	0.157	0.060 $\pm$ 0.023 (38%)	0.003	0.143	0.033 $\pm$ 0.021 (64%)

<sup>a</sup>Coefficient of variation (CV, in units of %), calculated as 100\*(SD-to-Mean ratio), is also shown.

coefficients than those observed in the northern hemisphere (Table 2). At temperate latitudes, the North Western Mediterranean Sea shows high  $K_{bio}(\lambda)$  coefficients close to those observed in the North Atlantic subpolar gyre (Table 2; Figure 3), while values close to those found in the Southern Ocean are observed in other subbasins of the region (Table 2; Figure 3). The Eastern Mediterranean Sea (together with the Red Sea) shows lower  $K_{bio}(\lambda)$  coefficients than those in the western part, especially in the Levantine Sea (Table 2). The subtropical gyres and their surrounding areas have the lowest  $K_{bio}(\lambda)$ , with observed values of  $0.013 \pm 0.006$  and  $0.009 \pm 0.004 m^{-1}$  in the South Pacific, and  $0.013 \pm 0.005$  and  $0.007 \pm 0.004 m^{-1}$  in the South Atlantic for  $K_{bio}(380)$  and  $K_{bio}(490)$  coefficients, respectively (Table 2; Figure 3).

The analysis of the average distance of each region from, and the results of the parallelism tests for regression coefficients with respect to the *Morel et al.* [2007b] relationship (equation (5)) evidence regional deviations from the mean statistical relationship. In Figures 4 and 5, each of the 25 selected regions is displayed

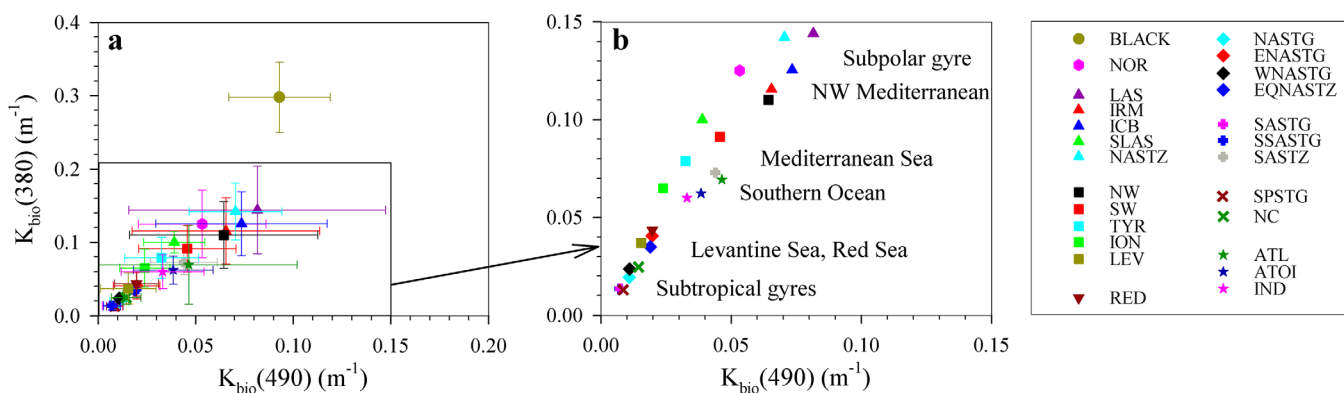


**Figure 3.** (a) Average  $K_{bio}(380)$  values ( $\pm$  standard deviation) as a function of the average  $K_{bio}(490)$  coefficients ( $\pm$  standard deviation) for the 25 geographic areas (see Table 1 for abbreviations); (b) as in Figure 3a but only for open ocean waters.

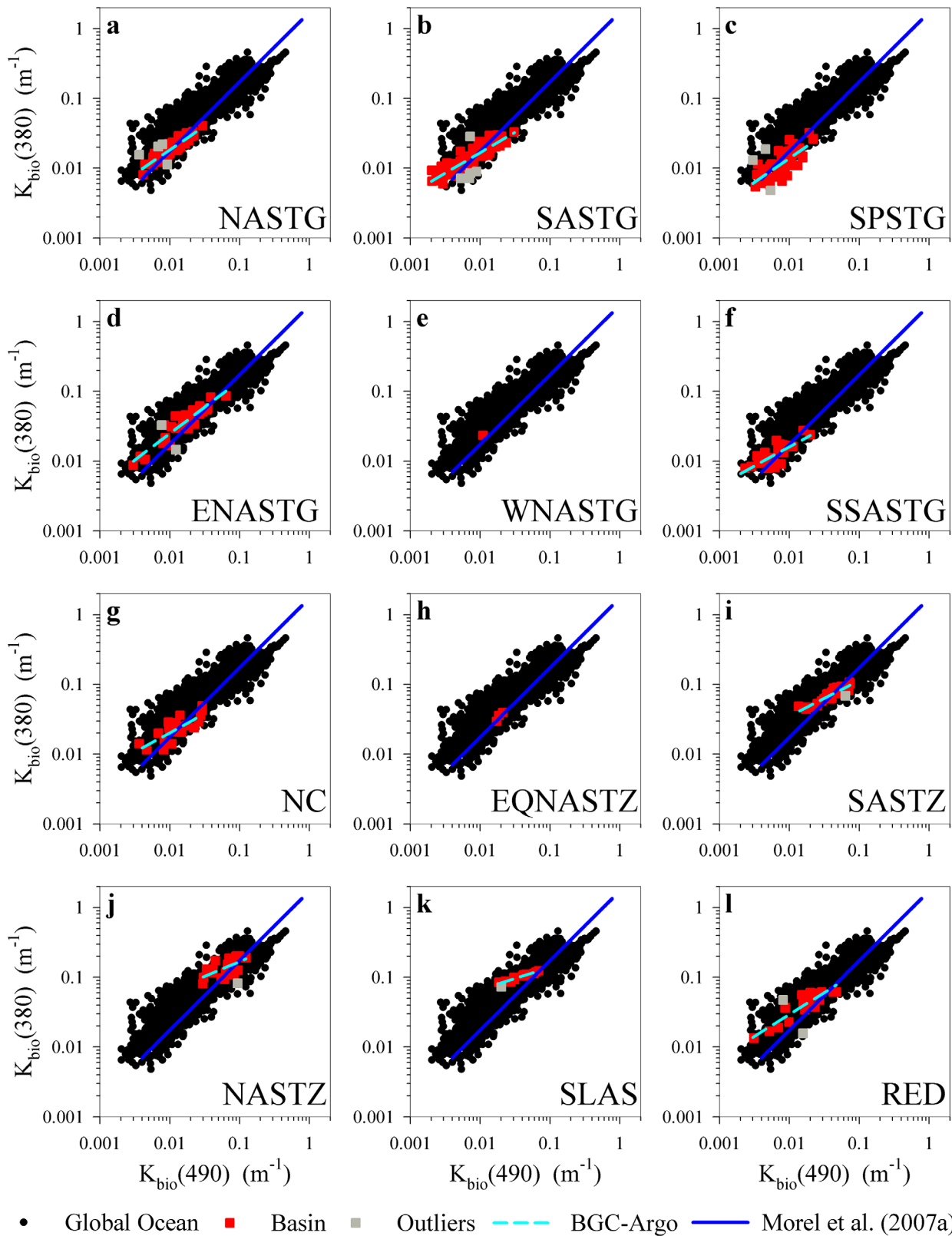


**Figure 4.** Log-log plot of  $K_{\text{bio}}(380)$  as a function of  $K_{\text{bio}}(490)$  for nonanomalous regions as compared to the global ocean represented by the BGC-Argo database. For each region, the power law fit and outliers removed for the computation are shown (see Table 3 for statistics). In each plot, previous regression line from *Morel et al.* [2007b] is shown for comparison and limited to the range of  $K_{\text{bio}}(490)$  values found in that study.

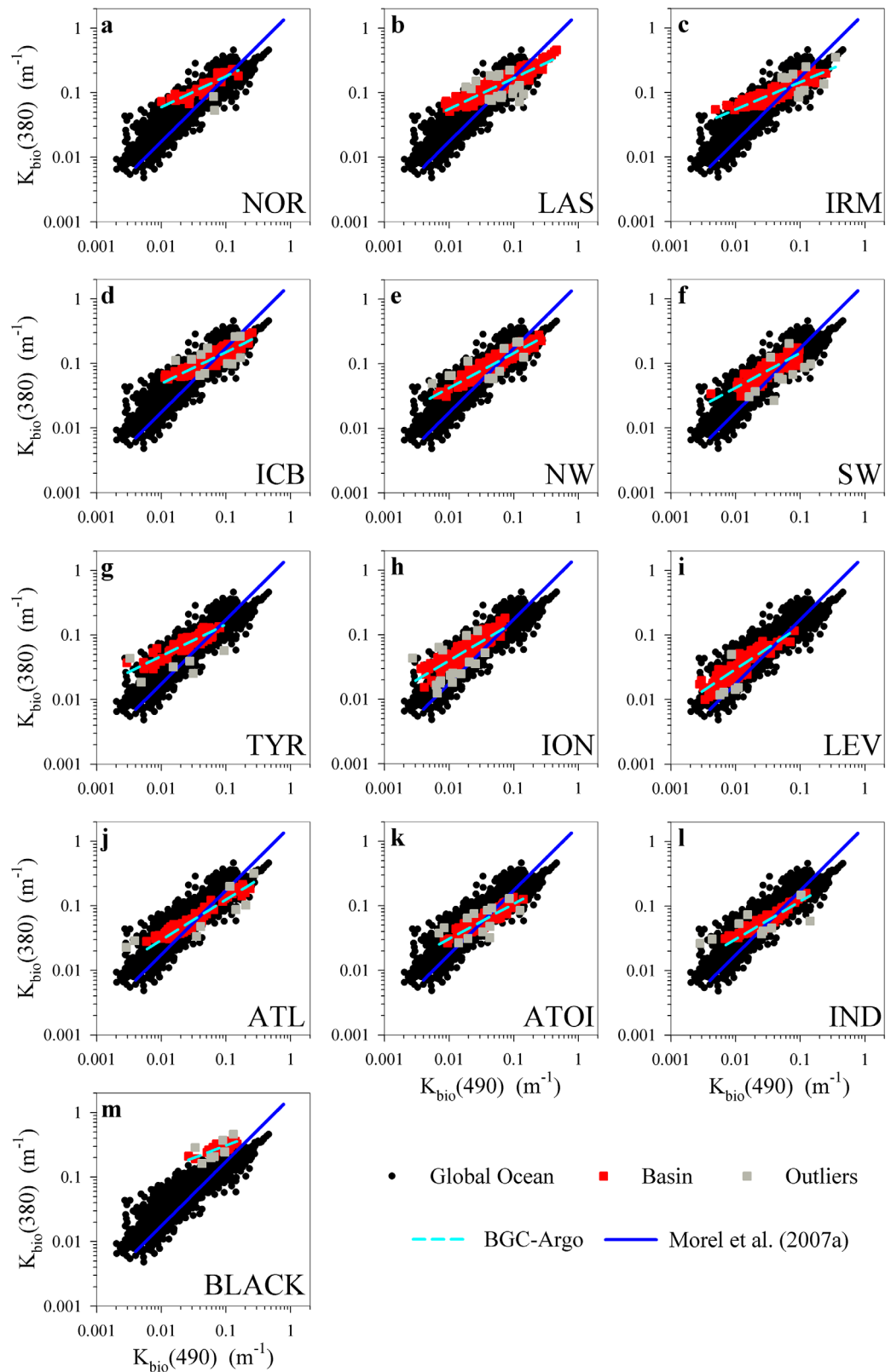


**Figure 5.** As Figure 4 but for regions characterized by bio-optical anomalies. For each region, the power law fit and outliers removed for the computation are shown (see Table 4 for statistics). In each plot, previous regression line from *Morel et al.* [2007b] is shown for comparison and limited to the range of  $K_{bio}(490)$  values found in that study.

**Table 3.** Statistics of Linear Regressions on Log-Transformed  $K_{bio}(\lambda)$  Quantities for Nonanomalous Open Ocean Waters Shown in Figure 4<sup>a</sup>

Region	Basin	N	$K_{bio}(380) = A * K_{bio}(490)^B$		$r^2$
			A	B	
North Atlantic subpolar gyre	South Labrador Sea	14	0.286 (±0.037)	0.316 (±0.026)	0.92 <sup>b</sup>
	Transition zone	24	0.443 (±0.140)	0.422 (±0.117)	0.34 <sup>ns</sup>
North Atlantic subtropical gyre	Subtropical gyre	63	0.419 (±0.078)	0.680 (±0.039)	0.83 <sup>b</sup>
	Eastern subtropical gyre	35	0.818 (±0.088)	0.758 (±0.049)	0.87 <sup>b</sup>
Red Sea	Red Sea	20	0.526 (±0.121)	0.627 (±0.068)	0.82 <sup>b</sup>
South Atlantic Ocean	Subtropical gyre	85	0.246 (±0.071)	0.584 (±0.032)	0.80 <sup>b</sup>
	South subtropical gyre	23	0.200 (±0.224)	0.547 (±0.101)	0.56 <sup>b</sup>
South Pacific Ocean	Transition Zone	30	0.371 (±0.056)	0.513 (±0.040)	0.85 <sup>b</sup>
	Subtropical gyre	42	0.324 (±0.204)	0.685 (±0.097)	0.55 <sup>b</sup>
	New Caledonia	23	0.254 (±0.181)	0.550 (±0.095)	0.60 <sup>b</sup>

<sup>a</sup>N is the number of measurements after removal of outliers and used for linear regression analysis (see section 2.4 for details). In parentheses, standard errors of linear regression coefficients on log-transformed data are reported. Regression statistics for the regions WNASTG and EQNASTZ in the North Atlantic Ocean are not shown because of the insufficient number of data.

<sup>b</sup>Highly significant determination coefficients ( $r^2$ ),  $p < 0.01$ ; <sup>ns</sup> not significant  $r^2$  values.

against the rest of the data within the database and the relationship described by *Morel et al.* [2007b] is also shown for comparison.

According to the observations by *Morel et al.* [2007a] in the South Pacific Ocean, all the subtropical gyres and the surrounding areas (Table 1) included in the BGC-Argo database are homogeneously distributed around the *Morel et al.* [2007b]'s model and no significant deviations are observed (Figures 4a–4j; Table 3). Hence, no bio-optical anomalies are found for these regions, as well as in the South Labrador and Red seas (Figures 4k and 4l; Table 3). More importantly, given the strong influence of ultraoligotrophic to oligotrophic environments in the mean statistical relationship [*Morel et al.*, 2007b], the observed results for subtropical gyres and the surrounding areas confirm the consistency between the apparent optical properties measured by the autonomous BGC-Argo floats and those measured during traditional oceanographic cruises under an operator's control and suitable meteorological conditions.

Bio-optical anomalies of  $K_{bio}(\lambda)$  coefficients are observed in the Norwegian Sea (Figure 5a), the North Atlantic subpolar gyre (Figures 5b–5d), the Mediterranean Sea (Figures 5e–5i), and in the Southern Ocean (Figures 5j–5l). These results agree with the previous observations on  $K_{bio}(\lambda)$  coefficients by *Morel et al.* [2007a] for the Mediterranean Sea, and with the analysis by *Szeto et al.* [2011] on reflectance band ratios vs chlorophyll *a* in the Atlantic and Southern Oceans. Separate linear regressions on log-transformed attenuation coefficients at 380 and 490 nm (Figure 5; Table 4) reveal that regional relationships significantly differ from

**Table 4.** Statistics of Linear Regressions on Log-Transformed  $K_{bio}(\lambda)$  Quantities for the Black Sea and Open Ocean Waters Characterized by Bio-Optical Anomalies and Shown in Figure 5<sup>a</sup>

Region	Basin	N	$K_{bio}(380) = A * K_{bio}(490)^B$		$r^2$
			A	B	
Arctic Sea	Norwegian Sea	40	0.541 (±0.051)	0.478 (±0.037)	0.81 <sup>b</sup>
North Atlantic subpolar gyre	Labrador Sea	479	0.505 (±0.011)	0.477 (±0.009)	0.86 <sup>b</sup>
	Irminger Sea	201	0.386 (±0.018)	0.425 (±0.013)	0.84 <sup>b</sup>
	Iceland Basin	233	0.459 (±0.018)	0.486 (±0.015)	0.82 <sup>b</sup>
Western Mediterranean Sea	Northwestern	216	0.510 (±0.018)	0.542 (±0.013)	0.89 <sup>b</sup>
	Southwestern	161	0.506 (±0.031)	0.540 (±0.021)	0.80 <sup>b</sup>
	Tyrrhenian Sea	88	0.452 (±0.036)	0.490 (±0.023)	0.84 <sup>b</sup>
Eastern Mediterranean Sea	Ionian Sea	229	0.609 (±0.033)	0.593 (±0.020)	0.80 <sup>b</sup>
	Levantine Sea	87	0.623 (±0.060)	0.662 (±0.030)	0.85 <sup>b</sup>
Southern Ocean	Atlantic sector	120	0.526 (±0.024)	0.626 (±0.015)	0.94 <sup>b</sup>
	Atlantic to Indian sector	215	0.374 (±0.023)	0.544 (±0.016)	0.85 <sup>b</sup>
	Indian sector	190	0.457 (±0.024)	0.586 (±0.016)	0.88 <sup>b</sup>
Black Sea	Black Sea	74	0.736 (±0.031)	0.378 (±0.029)	0.69 <sup>b</sup>

<sup>a</sup>N is the number of measurements after removal of outliers and used for linear regression analysis (see section 2.4 for details). In parentheses, standard errors of linear regression coefficients on log-transformed data are reported.

<sup>b</sup>Highly significant determination coefficients ( $r^2$ ),  $p < 0.01$ .

the model by *Morel et al.* [2007b] with  $K_{\text{bio}}(380)$  values generally above the curve, except for the highest  $K_{\text{bio}}(490)$  coefficients (Figure 5; Table 4).

The Black Sea is identified as an anomalous region. All  $K_{\text{bio}}(\lambda)$  coefficients measured in that area clearly differentiate from the other examined zones and the *Morel et al.* [2007b]'s model (Figure 5m; Table 4). Previous studies classify the Black Sea as a Case 2 water type [*Kopelevich et al.*, 2008; *Zibordi et al.*, 2013] while the model by *Morel et al.* [2007b] represents only open ocean Case 1 waters [*Morel and Prieur*, 1977]. This specificity is essentially related to the high concentrations of the colored fraction of dissolved organic pool [*Suetin et al.*, 2002; *Kopelevich et al.*, 2008], confirmed also by the observations of a BGC-Argo float at the surface (FDOM  $\sim 4$  ppb). Indeed, owing to river freshwater inflows [*Cauwet et al.*, 2002; *Margolin et al.*, 2016], the concentration of dissolved organic carbon in this basin is twice as high as in the open ocean [*Ducklow et al.*, 2007].

### 3.3. Temporal Variability and Sources of Bio-Optical Anomalies in Open Ocean Waters

Thanks to the sampling mode of BGC-Argo floats, anomalous open ocean waters were investigated for more than 1 year. This provides—for the first time—an assessment of the temporal optical variability of several regions with respect to the mean statistical relationships. Monthly climatologies of the  $K_{\text{bio}}(380)/K_{\text{bio}}(490)$  and FDOM/Chl ratios, and of the bio-optical model by *Morel et al.* [2007b], are analyzed for this purpose, except for the Norwegian Sea because of FDOM measurement unavailability. In view of this examination, and given that geographically close regions behave similarly, the remaining 11 open ocean waters with bio-optical anomalies are grouped into four major areas (Figure 6): (i) the North Atlantic subpolar gyre (i.e., Labrador Sea, Irminger Sea, Iceland Basin); (ii) the Western Mediterranean Sea (Tyrrhenian Sea, Northern and Southern basins); (iii) the Eastern Mediterranean Sea (Ionian and Levantine basins); and (iv) the Southern Ocean (Atlantic and Indian sectors).

In the North Atlantic subpolar gyre, the largest deviations from the mean statistical relationship [*Morel et al.*, 2007b] are recorded in winter and autumn with  $K_{\text{bio}}(380)/K_{\text{bio}}(490)$  ratios up to  $4.38 \pm 1.84$  in January and  $3.95 \pm 1.01$  in December (Figure 6a). Deviations strongly decrease in spring and summer showing  $K_{\text{bio}}(380)/K_{\text{bio}}(490)$  ratios close to the *Morel et al.* [2007b]'s model (Figure 6a). This temporal variation is explained by dynamics of the phytoplankton chlorophyll *a* concentration and its relation with the dissolved organic matter (Figure 6b). The climatology of the FDOM/Chl ratios is correlated with that of the  $K_{\text{bio}}(380)/K_{\text{bio}}(490)$  ratio ( $r = 0.59$ ) and no time shift is observed among their respective maxima and minima (Figure 6c). Furthermore, the observed temporal trend of the bio-optical anomaly is essentially driven by variations in chlorophyll *a* concentration rather than in FDOM. The North Atlantic subpolar gyre is a region characterized every year by a massive phytoplankton bloom, typically of diatoms, starting in March and ending at the end of the summer [*Longhurst*, 2007; *Alkire et al.*, 2012], and that represents one of the major planetary events of carbon export to the deep ocean [*Martin et al.*, 1993; *Briggs et al.*, 2011]. The BGC-Argo floats deployed in this region detected the bloom occurrence with Chl concentration up to  $12 \text{ mg m}^{-3}$  within the first optical depth, higher by about three orders of magnitude than the concentrations observed in winter ( $0.02 \text{ mg m}^{-3}$ ). On the contrary, FDOM remained approximately constant during all the year (average value of  $1.52 \pm 0.11$  ppb; Figure 6b). According to the indications of *Nelson and Gaultz* [2016] on the type of fluorescent dissolved organic material detected by a given excitation/emission couple of wavelengths, fluorimeters installed on BGC-Argo floats provide a measurement of aged humic material rather than of freshly produced substances [*Stedmon and Nelson*, 2015]. This suggests the occurrence of a background of humic dissolved organic material in this area, likely due to the high vertical mixing occurring in winter causing the upwelling of aged organic matter from deep reservoirs.

Large deviations of the  $K_{\text{bio}}(380)/K_{\text{bio}}(490)$  ratios from the mean statistical relationship [*Morel et al.*, 2007b] characterize the Western Mediterranean Sea after the spring bloom (Figure 6d). These deviations are notably remarkable during summertime when values up to  $3.90 \pm 0.95$  are reached (Figure 6d). Analogously to the North Atlantic subpolar gyre, no time shift and significant correlation ( $r = 0.49$ ) are observed between the time-series of  $K_{\text{bio}}(380)/K_{\text{bio}}(490)$  and FDOM/Chl ratios (Figures 6e–f). The persistent postbloom anomaly is generated by higher than expected FDOM values for low chlorophyll *a* concentrations, even in summer and autumn when FDOM values decrease because of photochemical degradation (Figure 6e). This statement is consistent also with recent observations in the region [*Organelli et al.*, 2014, 2016a, *Pérez et al.*, 2016]. Indeed, despite the clear seasonal dynamics of CDOM and NAP light absorption coefficients

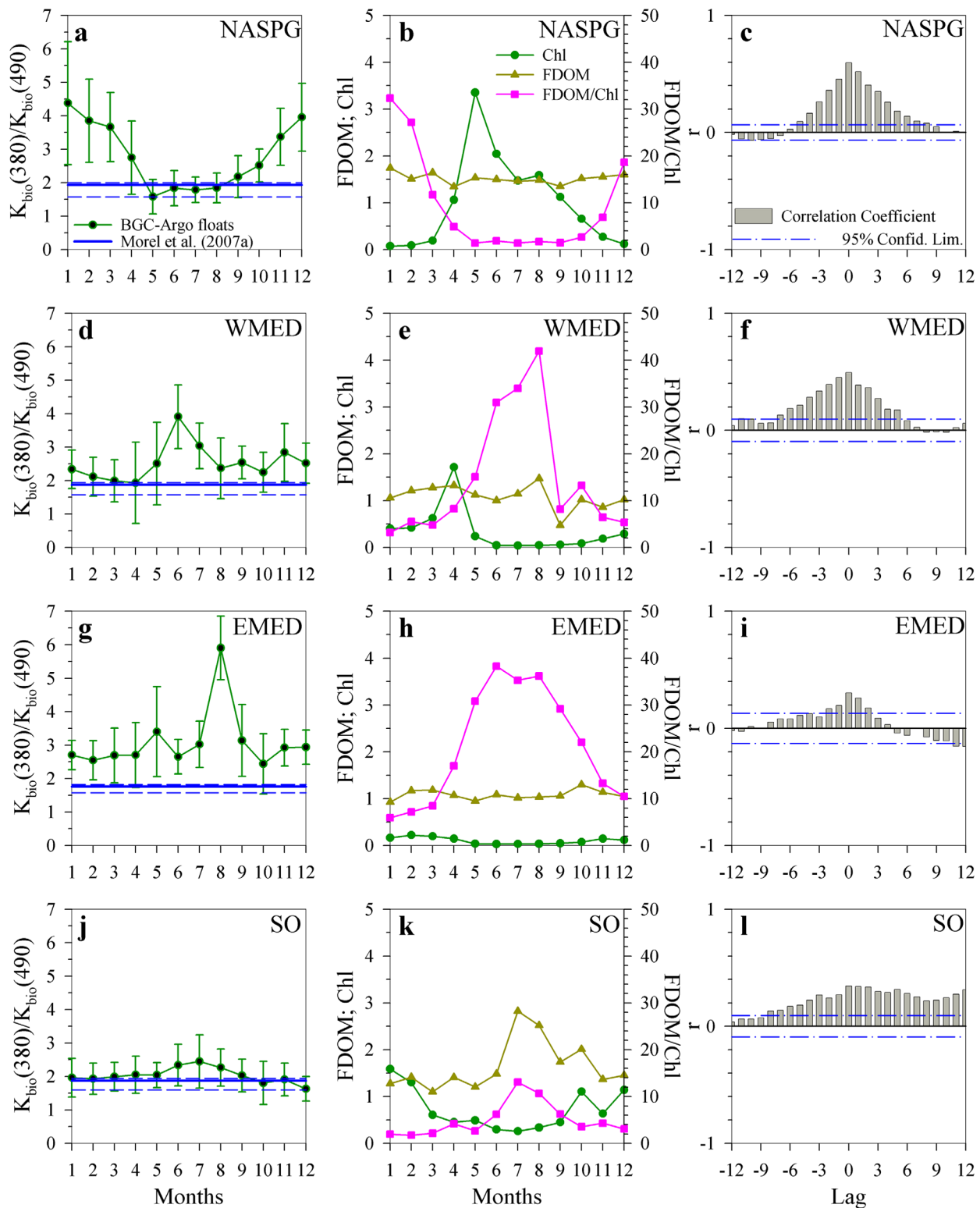


**Figure 6.** Monthly climatology of (left column)  $K_{bio}(380)/K_{bio}(490)$  ratios derived from BGC-Argo float measurements and from the Morel et al. [2007b] model; (central column) FDOM and chlorophyll *a* concentrations (ppb and  $mg\ m^{-3}$ , respectively) and ratio (ppb  $m^3\ mg^{-1}$ ). Right column plots show cross-correlation coefficient (*r*) between  $K_{bio}(380)/K_{bio}(490)$  and FDOM/Chl ratios. Climatologies are for the following areas: (a–c) the North Atlantic subpolar Gyre (NASPG); (d–f) the Western Mediterranean Sea (WMED); (g–i) the Eastern Mediterranean Sea (EMED); and (j–l) the Southern Ocean (SO). In left column plots, the solid line represents the mean  $K_{bio}(380)/K_{bio}(490)$  ratio as derived from the Morel et al. [2007b] model applied in the range of chlorophyll *a* concentrations measured by BGC-Argo floats within a given region. Dashed lines represent the boundaries of the  $K_{bio}(380)/K_{bio}(490)$  ratios as derived from the Morel et al. [2007b] model and the minimum and maximum of the measured chlorophyll *a* range.

characterizing the Western Mediterranean basin, CDOM remains the main optically significant substance dominating the light absorption budget in the UV and blue light spectrum during most of the year except during the bloom [Organelli *et al.*, 2014].

In the Eastern Mediterranean basin, deviations from the bio-optical relationship established by Morel *et al.* [2007b] are observed during all the year and are enhanced in summer with values up to  $5.90 \pm 0.94$  (Figure 6g). The significant correlation between the time-series of  $K_{\text{bio}}(380)/K_{\text{bio}}(490)$  and FDOM/Chl ratios ( $r = 0.30$ ), besides the lack of a time-shift between them, highlights the relevance of the dynamics of the dissolved organic material with respect to phytoplankton chlorophyll. The Eastern Mediterranean basin is an oligotrophic region with no bloom occurrence and consequently the lowest chlorophyll *a* concentrations observed in the whole Mediterranean Sea during most of the year [Bosc *et al.*, 2004; D'Ortenzio and Ribera d'Alcalà, 2009]. Despite these low Chl concentrations, also detected by BGC-Argo floats (Figure 6h), FDOM values are close to those observed in the western part (Figure 6e) varying from 0.92 to 1.30 ppb (Figure 6h). In summer, only a slight decrease in FDOM is observed as a consequence of the photochemical degradation [Xing *et al.*, 2014a] while chlorophyll *a* concentrations decrease to about  $0.03 \text{ mg m}^{-3}$  (Figure 6h).

In the Southern Ocean,  $K_{\text{bio}}(380)/K_{\text{bio}}(490)$  ratio always remains close to the mean statistical relationship [Morel *et al.*, 2007b], except in winter when it increases up to  $2.45 \pm 0.80$  (Figure 6j). The FDOM/Chl ratios also increase in parallel with the  $K_{\text{bio}}(\lambda)$  ratio (Figures 6k and 6l). This is mainly due to a winter FDOM increase in correspondence to low chlorophyll *a* values characterizing this area from March to September (Figure 6k). Analogously to the North Atlantic subpolar gyre, this increase of FDOM could be a consequence of the release of aged humic organic material by the deep ocean reservoirs owing to advection processes [Nelson *et al.*, 2010]. In the Southern Ocean, deviations from the Morel *et al.* [2007b]'s model (as well as the variability of FDOM/Chl ratios) are, however, less apparent compared to the other examined regions (Figure 6). This suggests a weaker effect of the colored dissolved organic matter than observed in other anomalous open ocean waters.

### 3.4. Other Sources of Bio-Optical Anomalies: Optical Properties of Phytoplankton Communities and Particle Light Backscattering

A particular physiological state and structure of the phytoplankton community, in response to changes in environmental conditions such as temperature, nutrient, and light availability, may impact the phytoplankton light absorption coefficients and thus the attenuation of downward irradiance in the water column. This was early observed in the Southern Ocean and polar regions where the cellular pigment packaging of the algal communities was reported to be more important than for communities from low latitudes [Mitchell and Holm-Hansen, 1991; Mitchell, 1992]. The increase of intracellular pigment contents induced by photoacclimation to low light can actually increase the so-called "packaging effect" [Morel and Bricaud, 1981] and lead to reduced chlorophyll specific phytoplankton light absorption [Sathyendranath *et al.*, 1987; Bricaud *et al.*, 2004] and diffuse attenuation coefficients in the blue part of the spectrum [Mitchell and Holm-Hansen, 1991]. Algal cell size also influences the pigment packaging [Morel and Bricaud, 1981; Bricaud *et al.*, 2004] and induces a flattening of the light absorption spectra [Ciotti *et al.*, 2002; Bricaud *et al.*, 2010]. However, because these spectral modifications of the light absorption coefficients simultaneously occur at 380 and 490 nm [Bricaud and Stramski, 1990], the analysis on  $K_{\text{bio}}$  ratios presented in the previous sections avoids evaluating thoroughly the influence of phytoplankton community and its optical properties on the bio-optical anomalies identified within the BGC-Argo database.

To evaluate this influence, the variations of  $K_{\text{bio}}(490)$  coefficients, and thus of the phytoplankton light absorption, as a function of chlorophyll *a* concentration are shown in Figure 7 and compared to the mean statistical relationship as described by Morel *et al.* [2007b]. The relationship based on BGC-Argo float data can be expressed as (standard errors of linear regression coefficients on log-transformed data in parentheses):

$$K_{\text{bio}}(490) = 0.063 (\pm 0.005) * \text{Chl}^{0.467 (\pm 0.007)} \quad (n=2454, r^2=0.62) \quad (7)$$

Differences appear between the BGC-Argo and the Morel *et al.* [2007b] relationships. It is important to keep in mind that the BGC-Argo Chl concentration is only a proxy of phytoplankton biomass as derived from fluorescence measurements. This implies that, besides some instrumental-induced bias [Roesler *et al.*, 2017], the fluorescence to chlorophyll concentration ratio potentially varies among regions as a consequence of

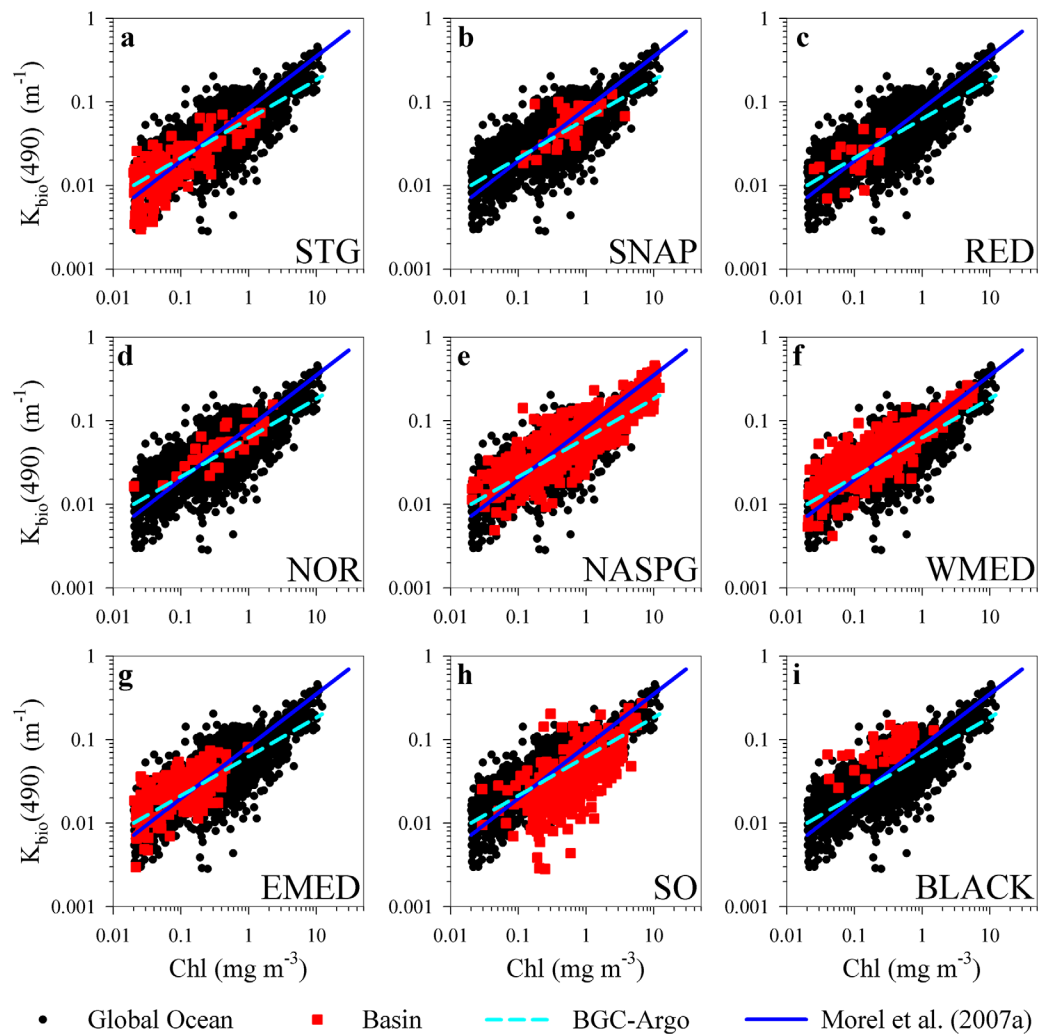


**Figure 7.** Log-log plot of  $K_{\text{bio}}(490)$  as a function of chlorophyll  $a$  concentration (Chl) for the following areas in comparison to the global ocean represented by the BGC-Argo database: (a) Subtropical gyres and surrounding areas (STG); (b) South Labrador Sea and transition zone (SNAP); (c) Red Sea (RED); (d) Norwegian Sea (NOR); (e) North Atlantic subpolar gyre (NASPG); (f) Western Mediterranean Sea (WMED); (g) Eastern Mediterranean Sea (EMED); (h) Southern Ocean (SO); and (i) Black Sea (BLACK). In each plot, the not-least square fit to the whole BGC-Argo database is shown. Previous regression line from Morel et al. [2007b] is also shown for comparison and limited to the range of Chl values found in that study.

changes in photophysiology, nutrient availability, growth, and taxonomic composition of algal communities [Cullen, 1982]. These sources of variability, together with errors associated to correction of the nonphotochemical quenching [Xing et al., 2012], can introduce some uncertainty in the measured Chl concentration that may not be taken in account by the factor 2 correction applied in this study.

Regional deviations from the mean statistical relationship [Morel et al., 2007b] are essentially observed for the Southern Ocean and Black Sea (Figures 7h–7i). The subtropical gyres as well as other nonanomalous areas are distributed around the Morel et al. [2007b] model (Figures 7a–7c). Among the regions with bio-optical anomalies, observations around Morel et al. [2007b] are also recorded for the Norwegian Sea, the North Atlantic subpolar gyre, and the Mediterranean Sea (Figures 7d–7g), that confirmed CDOM (with NAP) and its relationship with chlorophyll  $a$  as principal drivers of the observed anomalies in the  $K_{\text{bio}}(\lambda)$  coefficients (see section 3.3). It is worth also noting that low  $K_{\text{bio}}(490)$  variability around the Morel et al. [2007b] model is mainly observed for high Chl concentrations (Figure 7). This may be a consequence of the few data points available for this Chl range, but also of some similarity between algal communities and therefore absorption properties of actively growing cells. Instead, at lower Chl concentrations, variable environmental conditions that limit algal growth may strongly modify pigment composition, intracellular pigment

contents, and size structure. This will in turn increase the variability in light absorption properties, including  $K_{\text{bio}}(490)$ , among phytoplankton communities and regions [Bricaud *et al.*, 2004].

On the contrary, in the Southern Ocean,  $K_{\text{bio}}(490)$  coefficients are generally lower than predicted by the Morel *et al.* [2007b]'s model for a given chlorophyll *a* concentration (Figure 7h). In this area, Chl determination from fluorescence measurements might be more affected by natural variability of the fluorescence to Chl ratio, possibly as a consequence of a higher fluorescence quantum yield than in other regions [Falkowski and Kolber, 1995]. A sensitivity test using the regional calibration factor for the Southern Indian Ocean [ $3.46 \pm 0.35$ ; Roesler *et al.*, 2017] evidences, however, only small changes in the distribution of points (data not shown). This suggests that deviation of  $K_{\text{bio}}(490)$  coefficients with respect to the Morel *et al.* [2007b] relationship expresses the presence of a higher pigment packaging of phytoplankton communities in the Southern Ocean than observed in other areas. In support to this, communities chiefly composed of large phytoplankton cells and notably diatoms, nanoflagellates, or colonies of the small haptophyte *Phaeocystis* sp., dominate the austral phytoplankton community structure [Mitchell and Holm-Hansen, 1991; Uitz *et al.*, 2009; Wright *et al.*, 2010]. Moreover, all these communities show relevant modifications of their optical properties and in particular a reduction of the chlorophyll-specific light absorption as a consequence of light or iron stresses [Mitchell and Holm-Hansen, 1991; Mitchell *et al.*, 1991; Moisan and Mitchell, 1999; Sosik and Olson, 2002].

Differently from open ocean waters,  $K_{\text{bio}}(490)$  coefficients in the Black Sea are generally higher than predicted by the Morel *et al.* [2007b]'s model (Figure 7i) for a given chlorophyll *a* concentration. Although the phytoplankton communities in this region are mainly composed by micro and nanophytoplankton [Agirbas *et al.*, 2015 and references therein] and a reduced light absorption per unit of chlorophyll as due to a high pigment packaging should be expected, phytoplankton is generally a small fraction of the total particle light absorption [Chami *et al.*, 2005]. The high  $K_{\text{bio}}(490)$  coefficients observed by BGC-Argo floats are, thus, likely due to high contributions of colored nonalgal particles mainly of mineral nature.

The total nonwater attenuation coefficients at 490 nm also covary with the total particle light backscattering within the first optical depth (Figure 8; standard errors of linear regression coefficients on log-transformed data in parentheses):

$$K_{\text{bio}}(490) = 15.99 (\pm 0.041) * b_{\text{bp}}(700)^{0.896 (\pm 0.014)} \quad (n=2535, r^2=0.63) \quad (8)$$

Modifications in the particle light backscattering are first dependent on the total particle amount, second on the composition and refractive index, and last on the size, shape, and internal structure of the material [Morel and Bricaud, 1986; Morel and Ahn, 1991; Stramski and Kiefer, 1991; Aas, 1996; Twardowski *et al.*, 2001; Stramski *et al.*, 2004; Loisel *et al.*, 2007].

The correlation between  $K_{\text{bio}}(490)$  and  $b_{\text{bp}}(700)$  is evident at the highest latitudes (Figures 8b, 8d, 8e, 8h) and in the Western Mediterranean Sea (Figure 8f), with  $r^2$  values ranging between 0.31 and 0.71. In these regions, the varying contribution of the light backscattering coefficients mainly depends on strong modifications in particle concentrations observed over time [Antoine *et al.*, 2011; Cetinić *et al.*, 2012]. The increase of  $K_{\text{bio}}(490)$  with  $b_{\text{bp}}(700)$  coefficients suggests that, because  $b_{\text{bp}}(700)$  is a proxy of particulate organic carbon [POC; Cetinić *et al.*, 2012], phytoplankton light absorption is related both to Chl and POC concentrations. Variations in  $b_{\text{bp}}(700)$  coefficients in these areas also reflect changes in particle-size distribution [Kheireddine and Antoine, 2014] as well as modifications of the phytoplankton community composition, toward a taxonomical structure dominated by diatoms [Cetinić *et al.*, 2015] or highly scattering calcifying haptophytes [Xing *et al.*, 2014b]. As previously observed, changes in cell size and pigment composition can modify the phytoplankton absorption coefficients, and eventually the light attenuation, in the blue part of the light spectrum [Mitchell and Holm-Hansen, 1991; Bricaud *et al.*, 2004].

In the subtropical gyres, the Red and Eastern Mediterranean seas,  $K_{\text{bio}}(490)$  coefficients vary over more than one order of magnitude for a given  $b_{\text{bp}}(700)$  value and no significant relationships are generally observed (Figures 8a, 8c, 8g). The weak correlation between  $K_{\text{bio}}(490)$  and  $b_{\text{bp}}(700)$  is likely related to a combination of different causes. The variability in  $K_{\text{bio}}(490)$  coefficients could be first due to the presence of organic, living or detrital, particles of various nature (e.g., nonalgal particles, bacteria, heterotrophs) that, despite similar and low particle concentrations (i.e., small  $b_{\text{bp}}(700)$  values), absorb different blue light quantities [Bricaud *et al.*, 2010]. Alternatively, changes in the physiological status of a given phytoplankton community in

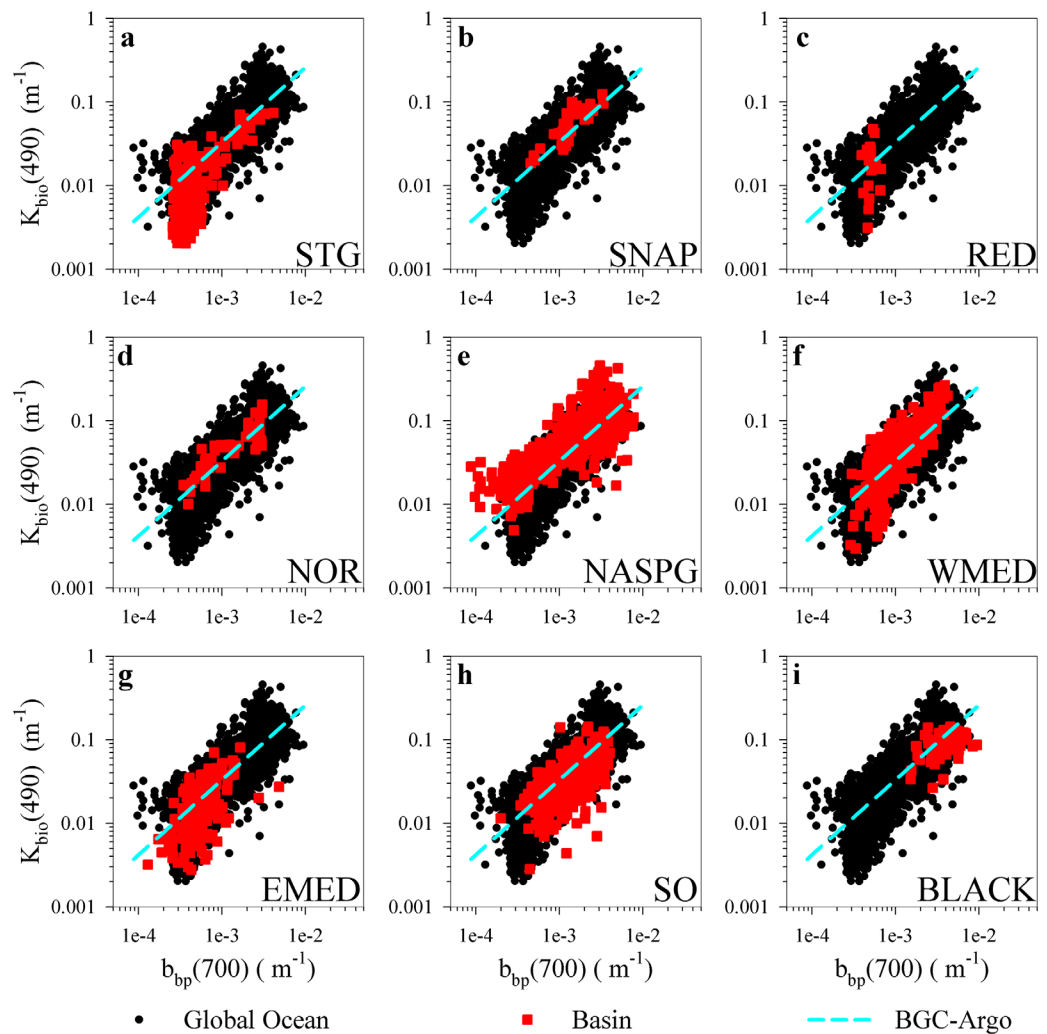


**Figure 8.** As in Figure 7 but for  $K_{\text{bio}}(490)$  as a function of  $b_{\text{bp}}(700)$  coefficients within the first optical depth. In each plot, the not-least square fit for the whole BGC-Argo database is shown.

response to light and nutrient availabilities could induce modifications in the phytoplankton pigment content and in the optical properties of the community [Sosik and Mitchell, 1995; Lazzara et al., 1996; Behrenfeld and Boss, 2003; Behrenfeld et al., 2005]. This can ultimately modify the attenuation of downward irradiance in the water column, despite an unchanged total amount of particles (and  $b_{\text{bp}}(700)$ ).

### 3.5. Global Spatiotemporal Distribution of Anomalies as Inferred From Diffuse Attenuation Coefficients for Downward Irradiance

The difference between the  $K_{\text{bio}}(380)/K_{\text{bio}}(490)$  ratio and the one estimated by the Morel et al. [2007b]'s model from the chlorophyll *a* concentration measured by BGC-Argo floats at each station can be used as an indicator for tracing bio-optical anomalies at the global scale and over time. From the analysis provided by the BGC-Argo float database, the presence of bio-optical anomalies shows a latitudinal gradient characterized by an increase from the Equator toward highest latitudes (Figure 9). This gradient has prominent features in winter (Figure 9a) and autumn (Figure 9d) while it is less marked in spring (Figure 9b) and summer (Figure 9c). Instead, at temperate latitudes, the Mediterranean and Black seas are characterized by bio-optical anomalies especially during summer (Figure 9c).

As discussed in previous sections, the colored fraction of the dissolved organic material, plus a contribution <20% of nonalgal particles [Siegel et al., 2002], are the main factors driving these deviations from previously established bio-optical models [i.e., Morel et al., 2007b]. However, an important aspect emerging from Figure 9

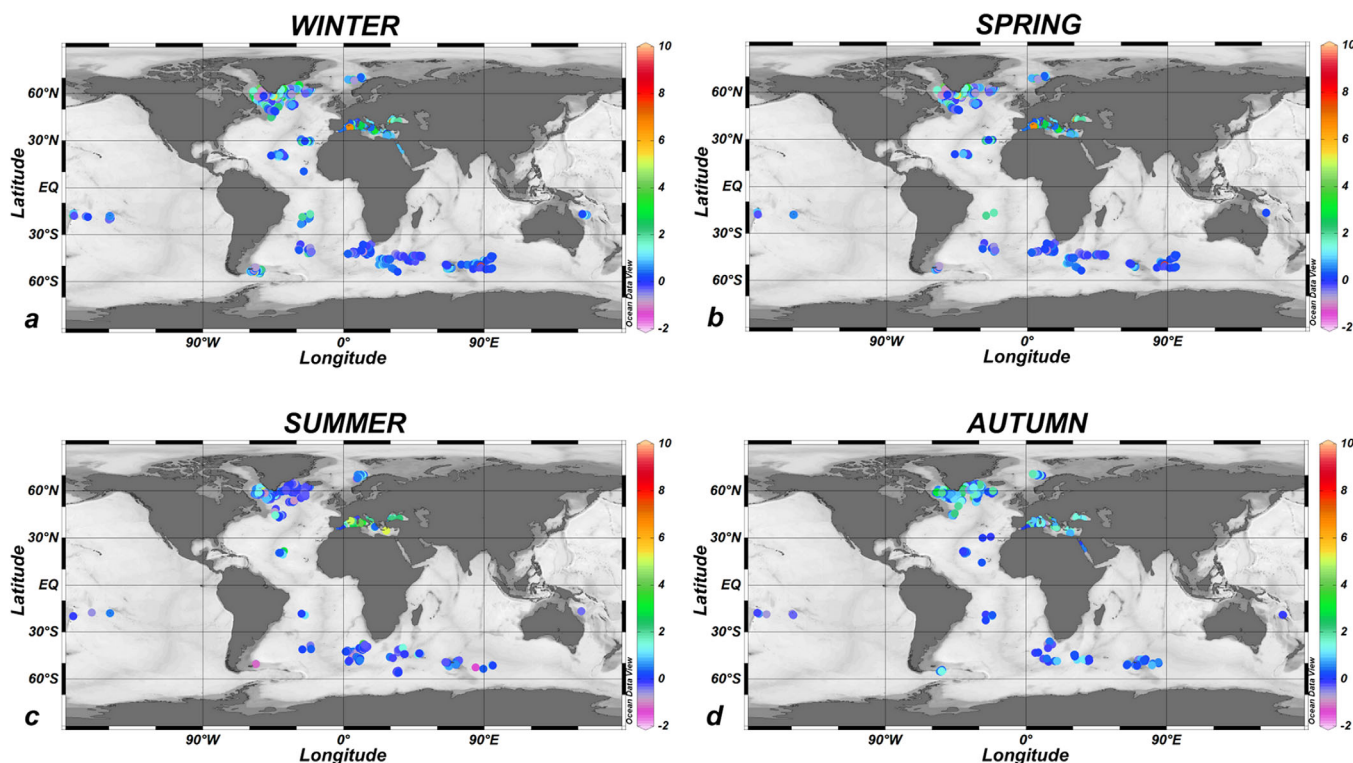


**Figure 9.** Bio-optical anomalies with respect to the mean statistical relationship by Morel *et al.* [2007b] as derived from the  $K_{\text{bio}}(380)/K_{\text{bio}}(490)$  ratios and chlorophyll *a* concentrations measured by BGC-Argo floats. Color bars indicate the difference between measured and modeled  $K_{\text{bio}}(380)/K_{\text{bio}}(490)$  ratios (dimensionless).

is that bio-optical anomalies can occur in a given region and time of the year in opposition to the average regional behavior. For example, high differences between the  $K_{\text{bio}}(380)/K_{\text{bio}}(490)$  ratios and those estimated by the Morel *et al.* [2007b]'s model are occasionally observed in the South Atlantic subtropical gyre in spring (Figure 9b) while differences close to 0 are found in the Mediterranean Sea during summer (Figure 9c). Such occurrences likely cause the large variability around the mean statistical relationships emerging from analyses above (Figure 6), and reveal particular events and biogeochemical processes that might deserve to be better addressed.

For example, unexpected low differences between measured and modeled  $K_{\text{bio}}(380)/K_{\text{bio}}(490)$  ratios could be related to changes in phytoplankton blue-absorbing accessory pigment concentrations and composition as a consequence of environmental stresses [Mitchell *et al.*, 1991; Moisan and Mitchell, 1999] or, alternatively, be a consequence of the presence of strongly absorbing mineral particles such as desert dusts deposited at the sea surface [Stramski *et al.*, 2001; Claustre *et al.*, 2002]. On the other side, high unexpected differences for a given region and time could be related to an increase of the relative contribution of well-colored organic detrital material as generated by picophytoplankton dominated communities that, thanks to generally high spectral slope values, have higher relative absorption in the UV than in the visible light [Bricaud *et al.*, 2010]. Finally, the occurrence of these bio-optical anomalies could also be a consequence of physical atmospheric and oceanic forcing that could generate high-frequency hydrodynamic variability (e.g., submesoscale circulation and deep vertical mixing), locally change the trophic environment and, in turn, modify the optical response.

#### 4. Summary and Conclusions

The main purpose of this study was to reexamine the regional variability of relationships between CDOM (together with nonalgal particles) and phytoplankton light absorption properties for the identification of those regions departing from previously established bio-optical models (i.e., bio-optical anomalies). Thanks to an extensive in situ database of diffuse attenuation coefficients of downward irradiance in the UV and

### Acknowledgments

We are grateful to the valuable work of Catherine Schmechtig (Ecce-Terra, France) for management of data acquired by the Biogeochemical Argo floats, Antoine Poteau (Laboratoire d'Océanographie de Villefranche, France) for pre and postdeployment verification and monitoring of float and sensor performance, and Grigor Obolensky (Euro-Argo ERIC, France) for deploying most of Biogeochemical Argo floats in many different oceanic areas. We warmly thank Bernard Gentili (Laboratoire d'Océanographie de Villefranche, France) for sharing data used to establish previous bio-optical relationships. This study was supported by the following research projects: remOcean (funded by the European Research Council, grant agreement 246777), NAOS (funded by the Agence Nationale de la Recherche in the frame of the French "Equipement d'avenir" program, grant agreement ANR J11R107-F), AtlantOS (funded by the European Union's Horizon 2020 research and innovation program, grant agreement 2014-633211), SOCLIM (funded by the Fondation BNP Paribas), E-AIMS (funded by the European Commission's FP7 project, grant agreement 312642), U.K. Bio-Argo (funded by the British Natural Environment Research Council, grant agreement NE/L012855/1), REOPTIMIZE (funded by the European Union's Horizon 2020 research and innovation program, Marie Skłodowska-Curie grant agreement 706781), Argo-Italy (funded by the Italian Ministry of Education, University and Research), and the French Bio-Argo program (Bio-Argo France; funded by CNES-TOSCA, LEFE Cyber, and GMMC). We thank the PIs of several BGC-Argo floats missions and projects: Kjell-Arne Mork (Institute of Marine Research, Norway; E-AIMS); Violeta Slabakova (Bulgarian Academy of Sciences, Bulgaria; E-AIMS); Emil Stanev (University of Oldenburg, Germany; E-AIMS); Pierre-Marie Poulain (National Institute of Oceanography and Experimental Geophysics, Italy; Argo-Italy); Sabrina Speich (Laboratoire de Météorologie Dynamique, France; Bio-Argo France); Virginie Thierry (Ifremer, France; Bio-Argo France); Pascal Conan (Observatoire Océanologique de Banyuls sur mer, France; Bio-Argo France); Laurent Coppola (Laboratoire d'Océanographie de Villefranche, France; Bio-Argo France); Anne Petrenko (Mediterranean Institute of Oceanography, France; Bio-Argo France); Jean-Baptiste Sallée (Laboratoire d'Océanographie et du Climat, France; Bio-Argo France); and Sorin Balan (GeoEcoMar, Romania).

visible derived from autonomous Biogeochemical Argo floats, sampled regions were grouped into three different groups according to their optical behavior within the first optical depth.

The first group only included the Black Sea, a water body characterized by very high CDOM contents. The second group was composed by the subtropical gyres in the Atlantic and South Pacific oceans, South Labrador, and Red seas. The optical properties of these latter areas were consistent with previously established models and no significant deviations were observed (i.e., no bio-optical anomalies). High latitude (Norwegian Sea, North Atlantic and Southern oceans) and temperate (Mediterranean Sea) seas formed the third group, in which the optical properties departed from the bio-optical model described by *Morel et al.* [2007b]. Furthermore, annual climatologies of the  $K_d(380)/K_d(490)$  ratios evidenced that the anomaly persisted almost all the year in the Mediterranean Sea, due to higher-than-average CDOM contribution to light absorption. In the North Atlantic subpolar gyre, it occurred only in wintertime, also due to the high CDOM content in these waters. In the Southern Ocean, the anomaly was related to high phytoplankton pigment packaging rather than to CDOM content. Particle light backscattering coefficients revealed the presence of highly refractive or well-colored organic detrital particles which also contributed to enhanced  $K_{bio}(\lambda)$  values.

Thanks to high-frequency measurements provided by BGC-Argo floats, the presence of single bio-optical anomalous events with respect to the regional average optical behavior can be also established. These occasional observations within a given region suggest that most of oceanic areas encounter, though with different frequency, all types of optical responses. Identification of such occurrences has surely implications on the application of bio-optical algorithms with in situ or satellite data for regional studies. More specifically, when an anomaly occurs, biogeochemical and bio-optical quantities might be retrieved with lower accuracy. More importantly, these occasional bio-optical anomalies may reveal the presence of particular events (e.g., submesoscale circulation, atmospheric fertilization) that underpin specific biogeochemical processes and may eventually impact the assessment of oceanic carbon fluxes and their implications on the Earth's climate.

The Biogeochemical Argo float network therefore represents an emerging observation system that, thanks to the several measured variables, helps better constraining the bio-optical behavior of the global ocean and the link with biogeochemical quantities. Moreover, float-derived variables such as  $K_d(\lambda)$  coefficients are, because of their physical nature (i.e.,  $E_d(\lambda)$  ratios), robust products with respect to any instrumental drift or biofouling issues. They could thus be implemented in programs of long-term data acquisition for identification of bio-optical anomalies and satellite bio-optical product validation. Biogeochemical Argo floats may therefore support and complement satellite ocean color measurements in next future, with activities ranging from quality-control and validation to data exploitation and modelling [IOCCG, 2015; *Biogeochemical-Argo Planning Group*, 2016 and references therein]. In the future, it could be also envisaged that thanks to an integrated observation system composed by Biogeochemical Argo optical measurements and geostationary satellite platforms, regional, and/or occasional bio-optical anomalies could be detected in near real time and used as proxies for identifying local biogeochemical processes. This could also help understanding better if the ocean and its optical properties have changed and/or are changing over the decades. Finally, thanks to the high spatial and temporal coverage, deciphering Biogeochemical Argo optical data can also allow to define future strategies of float deployment and oceanographic cruises. It will undoubtedly help reducing the undersampling bias characterizing ship-based observations and increasing the knowledge of ocean variability. This will represent a relevant contribution to the investigation and setting of regional bio-optical parameterizations aimed to improving satellite product retrievals in accuracy, as well as to the development of new bio-optical "global" standards (i.e., bio-optical relationships) against which we could compare optical and biogeochemical properties in different regions and maybe redefine current optical classifications of water bodies.

### References

- Aas, E. (1996), Refractive index of phytoplankton derived from its metabolite composition, *J. Plankton Res.*, 18, 2223–2249.
- Agirbas, E., A. M. Fezyoglu, U. Kopuz, and C. A. Llewellyn (2015), Phytoplankton community composition in the south-eastern Black Sea determined with pigments measured by HPLC-CHEMTAX analyses and microscopy cell counts, *J. Mar. Biol. Assoc. U. K.*, 95, 35–52, doi: 10.1017/S0025315414001040.
- Alkire, M. B., E. D'Asaro, C. Lee, M. J. Perry, A. Gray, I. Cetinic, N. Briggs, E. Rehm, E. Kallin, J. Kaiser, and A. González-Posada (2012), Estimates of net community production and export using high-resolution, Lagrangian measurements of  $O_2$ ,  $NO_3^-$ , and POC through the evolution of a spring diatom bloom in the North Atlantic, *Deep Sea Res., Part I*, 64, 157–174.

Collin Roesler (Bowdoin College, USA) and Emmanuel Boss (University of Maine, USA) are acknowledged for comments and discussion on data during the analysis. Steven G. Ackleson (NRL-DC, USA) and an anonymous reviewer are thanked for the constructive comments on a previous version of the manuscript. Biogeochemical Argo raw data used in this study are publicly available online (at <ftp://ftp.ifremer.fr/ifremer/argo/dac/coriolis>) and distributed as netCDF files. The quality-controlled database of bio-optical products within the first optical depth that supports conclusions is publicly available from SEANOE (SEA scieNtific Open data Edition) publisher [Organelli et al., 2016c]. No conflicts of interests are declared.

- Antoine, D., D. A. Siegel, T. Kostadinov, S. Maritorena, N. B. Nelson, B. Gentili, V. Vellucci, and N. Guillocheau (2011), Variability in optical particle backscattering in contrasting bio-optical oceanic regimes, *Limnol. Oceanogr.*, *56*(3), 955–973.
- Antoine, D., M. Babin, J.-F. Berthon, A. Bricaud, B. Gentili, H. Loisel, S. Maritorena, and D. Stramski (2014), Shedding light on the sea: André Morel's legacy to optical oceanography, *Annu. Rev. Mar. Sci.*, *6*, 15.1–15.21.
- Behrenfeld, M. J., and E. Boss (2003), The beam attenuation to chlorophyll ratio: An optical index of phytoplankton physiology in the surface ocean?, *Deep Sea Res., Part 1*, *50*, 1537–1549.
- Behrenfeld, M. J., E. Boss, D. A. Siegel, and D. M. Shea (2005), Carbon-based ocean productivity and phytoplankton physiology from space, *Global Biogeochem. Cycles*, *19*, GB1006, Ifremer, France, doi:10.1029/2004GB002299.
- Biogeochemical-Argo Planning Group (2016), *The Scientific Rationale, Design and Implementation Plan for a Biogeochemical-Argo Float Array*, edited by K. Johnson and H. Claustre, Ifremer, France, doi:10.13155/46601.
- Bosc, E., A. Bricaud, and D. Antoine (2004), Seasonal and interannual variability in algal biomass and primary production in the Mediterranean Sea, as derived from four years of SeaWiFS observations, *Global Biogeochem. Cycles*, *18*, GB1005, doi:10.1029/2003GB002034.
- Bosc, E., and W. S. Pegau (2001), Relationship of light scattering at an angle in the backward direction to the backscattering coefficient, *Appl. Opt.*, *40*(30), 5503–5507.
- Bricaud, A., and D. Stramski (1990), Spectral absorption coefficients of living phytoplankton and nonalgal biogenous matter: A comparison between Peru upwelling area and Sargasso Sea, *Limnol. Oceanogr.*, *35*, 562–582.
- Bricaud, A., A. Morel, and L. Prieur (1981), Absorption by dissolved organic matter of the sea (yellow substance) in the UV and visible domains, *Limnol. Oceanogr.*, *26*(1), 43–53.
- Bricaud, A., E. Bosc, and D. Antoine (2002), Algal biomass and sea surface temperature in the Mediterranean Basin: Intercomparison of data from various satellite sensors, and implications for primary production estimates, *Remote Sens. Environ.*, *81*, 163–178.
- Bricaud, A., H. Claustre, J. Ras, and K. Oubelkheir (2004), Natural variability of phytoplanktonic absorption in oceanic waters: Influence of the size structure of algal populations, *J. Geophys. Res.*, *109*, C11010, doi:10.1029/2004JC002419.
- Bricaud, A., M. Babin, H. Claustre, J. Ras, and F. Tièche (2010), Light absorption properties and absorption budget of Southeast Pacific waters, *J. Geophys. Res.*, *115*, C08009, doi:10.1029/2009JC005517.
- Briggs, N., M. J. Perry, I. Cetinic, C. Lee, E. D'Asaro, A. M. Gray, and E. Rehm (2011), High-resolution observations of aggregate flux during a sub-polar North Atlantic spring bloom, *Deep Sea Res., Part 1*, *58*, 1031–1039.
- Cauwet, G., G. Déliat, A. Krastev, G. Shtereva, S. Becquevort, C. Lancelot, A. Momzikoff, A. Saliot, A. Cociasu, and L. Popa (2002), Seasonal DOC accumulation in the Black Sea: A regional explanation for a general mechanism, *Mar. Chem.*, *79*, 193–205.
- Cetinic, I., M. J. Perry, N. T. Briggs, E. Kallin, E. A. D'Asaro, and C. M. Lee (2012), Particulate organic carbon and inherent optical properties during 2008 North Atlantic Bloom Experiment, *J. Geophys. Res.*, *117*, C06028, doi:10.1029/2011JC007771.
- Cetinic, I., M. J. Perry, E. D'Asaro, N. Briggs, N. Poulton, M. E. Sieracki, and C. M. Lee (2015), A simple optical index shows spatial and temporal heterogeneity in phytoplankton community composition during the 2008 North Atlantic Bloom Experiment, *Biogeosciences*, *12*, 2179–2194.
- Chami, M., E. B. Shybanov, T. Y. Churilova, G. A. Khomenko, M. E.-G. Lee, O. V. Martynov, G. A. Berseneva, and G. K. Korotaev (2005), Optical properties of the particles in the Crimea coastal waters (Black Sea), *J. Geophys. Res.*, *110*, C11020, doi:10.1029/2005JC003008.
- Ciotti, A. M., M. R. Lewis, and J. J. Cullen (2002), Assessment of the relationships between dominant cell size in natural phytoplankton communities and the spectral shape of the absorption coefficient, *Limnol. Oceanogr.*, *47*, 404–417.
- Claustre, H., and S. Maritorena (2003), The many shades of ocean blue, *Science*, *302*, 1514–1515.
- Claustre, H., A. Sciandra, and D. Valuot (2008), Introduction to the special section bio-optical and biogeochemical conditions in the South East Pacific in late 2004: The BIOSOPE program, *Biogeosciences*, *5*, 679–691.
- Claustre, H., A. Morel, S. B. Hooker, M. Babin, D. Antoine, K. Oubelkheir, A. Bricaud, K. Leblanc, B. Quéguiner, and S. Maritorena (2002), Is desert dust making oligotrophic waters greener?, *Geophys. Res. Lett.*, *29*(10), 1469, doi:10.1029/2001GL014056.
- Cullen, J. J. (1982), The deep chlorophyll maximum: Comparing vertical profiles of chlorophyll *a*, *Can. J. Fish. Aquat. Sci.*, *39*, 791–803.
- D'Ortenzio, F., and M. Ribera d'Alcalà (2009), On the trophic regimes of the Mediterranean Sea: A satellite analysis, *Biogeosciences*, *6*, 139–148.
- D'Ortenzio, F., S. Marullo, M. Ragni, M. Ribera d'Alcalà, and R. Santoleri (2002), Validation of empirical SeaWiFS algorithms for chlorophyll-*a* retrieval in the Mediterranean Sea. A case study for oligotrophic seas, *Remote Sens. Environ.*, *82*, 79–94.
- Ducklow, H. W., D. A. Hansell, and J. A. Morgan (2007), Dissolved organic carbon and nitrogen in the Western Black Sea, *Mar. Chem.*, *105*, 140–150.
- Falkowski, P. G., and Z. Kolber (1995), Variations in chlorophyll fluorescence yields in phytoplankton in the world oceans, *Aust. J. Plant Physiol.*, *22*, 341–355.
- Gordon, H. R. (1989), Can the Lambert-Beer law be applied to the diffuse attenuation coefficient of ocean water?, *Limnol. Oceanogr.*, *34*, 1389–1409.
- Gordon, H. R., and W. R. McCluney (1975), Estimation of the depth of sunlight penetration in the sea for remote sensing, *Appl. Opt.*, *14*, 413–416.
- Gordon, H. R., O. B. Brown, R. H. Evans, J. W. Brown, R. C. Smith, K. S. Baker, and D. K. Clark (1988), A semianalytic radiance model of ocean color, *J. Geophys. Res.*, *93*, 10,909–10,924.
- Huot, Y., and D. Antoine (2016), Remote sensing reflectance anomalies in the ocean, *Remote Sens. Environ.*, *184*, 101–111.
- IOCCG (2011), Bio-optical sensors on Argo floats, *IOCCG Rep. Ser. 11*, 89 pp., Dartmouth, Canada.
- IOCCG (2015), *Proceedings of the 2015 International Ocean Colour Science Meeting*, 45 pp., IOCCG, San Francisco, Calif. [Available at <http://iocs.ioccg.org>]
- Johnson, K. S., and H. Claustre (2016), Bringing biogeochemistry into the Argo age, *Eos*, *97*, doi:10.1029/2016E0062427.
- Kheiredine, M., and D. Antoine (2014), Diel variability of the beam attenuation and backscattering coefficients in the northwestern Mediterranean Sea (BOUSSOLE site), *J. Geophys. Res. Oceans*, *119*, 5465–5482, doi:10.1002/2014JC010007.
- Kiefer, D. A. (1973), Fluorescence properties of natural phytoplankton populations, *Mar. Biol.*, *22*, 263–269.
- Kopelevich, O. V., V. I. Burenkov, and S. V. Sheberstov (2008), Case studies of optical remote sensing in the Barent Sea, Black Sea and Caspian Sea, in *Remote Sensing of the European Seas*, edited by V. Barale and M. Gade, pp. 53–66, Springer Science+Business Media BV, Dordrecht, Netherlands.
- Lazzara, L., A. Bricaud, and H. Claustre (1996), Spectral absorption and fluorescence excitation properties of phytoplankton populations at a mesotrophic and an oligotrophic site in the tropical North Atlantic (EUMELI program), *Deep Sea Res., Part 1*, *43*(8), 1215–1240.

- Loisel, H., X. Mériaux, J.-F. Berthon, and A. Poteau (2007), Investigation of the optical backscattering to scattering ratio of marine particles in relation to their biogeochemical composition in the eastern English Channel and southern North Sea, *Limnol. Oceanogr.*, *52*, 739–752.
- Longhurst, A. R. (2007), The Atlantic Ocean, in *Ecological Geography of the Sea*, 2nd ed., edited by A. R. Longhurst, pp. 131–273, Academic, Burlington.
- Margolin, A. R., L. J. A. Gerringa, D. A. Hansell, and M. J. A. Rijkenberg (2016), Net removal of dissolved organic carbon in the anoxic waters of the Black Sea, *Mar. Chem.*, *183*, 13–24.
- Martin, J. H., S. E. Fitzwater, R. M. Gordon, C. N. Hunter, and S. J. Tanner (1993), Iron, primary production and carbon–nitrogen flux studies during the JGOFS North Atlantic Bloom Experiment, *Deep Sea Res., Part II*, *40*(1–2), 115–134.
- Matsuoka, A., V. Hill, Y. Huot, M. Babin, and A. Bricaud (2011), Seasonal variability in the light absorption properties of western Arctic waters: Parameterization of the individual components of absorption for ocean color applications, *J. Geophys. Res.*, *116*, C02007, doi:10.1029/2009JC005594.
- Mitchell, B. G. (1992), Predictive bio-optical relationships for polar oceans and marginal ice zones, *J. Mar. Syst.*, *3*, 91–105.
- Mitchell, B. G., and O. Holm-Hansen (1991), Bio-optical properties of Antarctic Peninsula waters: Differentiation from temperate ocean models, *Deep Sea Res., Part A*, *38*, 1009–1028.
- Mitchell, B. G., E. A. Brody, O. Holm-Hansen, C. McClain, and J. Bishop (1991), Light limitation of phytoplankton biomass and macronutrient utilization in the Southern Ocean, *Limnol. Oceanogr.*, *36*, 1662–1677.
- Moisan, T. A., and B. G. Mitchell (1999), Photophysiological acclimation of *Phaeocystis antarctica* Karsten under light limitation, *Limnol. Oceanogr.*, *44*(2), 247–258.
- Morel, A. (1988), Optical modeling of the upper ocean in relation to its biogenous matter content (Case I waters), *J. Geophys. Res.*, *93*, 10,749–10,768.
- Morel, A., and Y.-H. Ahn (1991), Optics of heterotrophic nanoflagellates and ciliates: A tentative assessment of their scattering role in oceanic waters compared to those of bacterial and algal cells, *J. Mar. Res.*, *49*, 177–202.
- Morel, A., and A. Bricaud (1981), Theoretical results concerning light absorption in a discrete medium, and application to specific absorption of phytoplankton, *Deep Sea Res., Part A*, *28*, 1375–1393.
- Morel, A., and A. Bricaud (1986), Inherent optical properties of algal cells including picoplankton: Theoretical and experimental results, *Can. Bull. Fish. Aquat. Sci.*, *214*, 521–559.
- Morel, A., and B. Gentili (2009a), A simple band ratio technique to quantify the colored dissolved and detrital organic material from ocean color remotely sensed data, *Remote Sens. Environ.*, *113*, 998–1011.
- Morel, A., and B. Gentili (2009b), The dissolved yellow substance and the shades of blue in the Mediterranean Sea, *Biogeosciences*, *6*, 2625–2636.
- Morel, A., and H. Loisel (1998), Apparent optical properties of oceanic waters: Dependence on the molecular scattering contribution, *Appl. Opt.*, *37*, 4765–4776.
- Morel, A., and S. Maritorena (2001), Bio-optical properties of oceanic waters: A reappraisal, *J. Geophys. Res.*, *106*, 7163–7180.
- Morel, A., and L. Prieur (1977), Analysis of variations in ocean color, *Limnol. Oceanogr.*, *22*, 709–722.
- Morel, A., H. Claustre, D. Antoine, and B. Gentili (2007a), Natural variability of bio-optical properties in Case 1 waters: Attenuation and reflectance within the visible and near-UV spectral domains, as observed in South Pacific and Mediterranean waters, *Biogeosciences*, *4*, 913–925.
- Morel, A., Y. Huot, B. Gentili, P. J. Werdell, S. B. Hooker, and B. A. Franz (2007b), Examining the consistency of products derived from various ocean color sensors in open ocean (Case 1) waters in the perspective of a multi-sensor approach, *Remote Sens. Environ.*, *111*, 69–88.
- Mueller, J. L., et al. (2003), Radiometric measurements and Data Analysis Protocols, in *Ocean Optics Protocols for Satellite Ocean Color Sensor Validation*, Rev. 4 vol. 3, NASA Tech. Mem. 2003–21621, edited by J. L. Mueller, G. S. Fargion, and C. R. McClain, NASA Goddard Space Flight Cent., Greenbelt, Md.
- Nelson, N. B., and J. M. Gauglitz (2016), Optical signatures of dissolved organic matter transformation in the global ocean, *Front. Mar. Sci.*, *2*, 118, doi:10.3389/fmars.2015.00118.
- Nelson, N. B., D. A. Siegel, C. A. Carlson, and C. M. Swan (2010), Tracing global biogeochemical cycles and meridional overturning circulation using chromophoric dissolved organic matter, *Geophys. Res. Lett.*, *37*, L03610, doi:10.1029/2009GL042325.
- Nelson, N. B., D. A. Siegel, C. A. Carlson, C. Swan, W. M. Smethie Jr., and S. Khatiwala (2007), Hydrography of chromophoric dissolved organic matter in the North Atlantic, *Deep Sea Res., Part I*, *54*, 710–731.
- Organelli, E., A. Bricaud, D. Antoine, and A. Matsuoka (2014), Seasonal dynamics of light absorption by Chromophoric Dissolved Organic Matter (CDOM) in the NW Mediterranean Sea (BOUSSOLE site), *Deep Sea Res., Part I*, *91*, 72–85, doi: 10.1016/j.dsr.2014.05.003.
- Organelli, E., A. Bricaud, B. Gentili, D. Antoine, and V. Vellucci (2016a), Retrieval of Colored Detrital Matter (CDM) light absorption coefficients in the Mediterranean Sea using field and satellite ocean color radiometry: Evaluation of bio-optical inversion models, *Remote Sens. Environ.*, *186*, 297–310, doi:10.1016/j.rse.2016.08.028.
- Organelli, E., H. Claustre, A. Bricaud, C. Schmechtig, A. Poteau, X. Xing, L. Prieur, F. D'Ortenzio, G. Dall'Olmo, and V. Vellucci (2016b), A novel near-real-time quality-control procedure for radiometric profiles measured by Bio-Argo floats: Protocols and performances, *J. Atmos. Oceanic Technol.*, *33*, 937–951, doi:10.1175/JTECH-D-15-0193.1.
- Organelli, E., M. Barbieux, H. Claustre, C. Schmechtig, A. Poteau, A. Bricaud, J. Uitz, F. D'Ortenzio, and G. Dall'Olmo (2016c), A global bio-optical database derived from Biogeochemical Argo float measurements within the layer of interest for field and remote ocean color applications, SEANOE, France. [Available at <http://doi.org/10.17882/47142>, accessed 14 Dec.]
- Pérez, G. L., M. Galí, S.-J. Royer, H. Sarmiento, J. M. Gasol, C. Marrasé, and R. Simó (2016), Bio-optical characterization of offshore NW Mediterranean waters: CDOM contribution to the absorption budget and diffuse attenuation of downwelling irradiance, *Deep Sea Res., Part I*, *114*, 111–127.
- Prieur, L., and S. Sathyendranath (1981), An optical classification of coastal and oceanic waters based on the specific spectral absorption curves of phytoplankton pigments, dissolved organic matter, and other particulate materials, *Limnol. Oceanogr.*, *26*(4), 671–689.
- Proctor, C. W., and C. S. Roesler (2010), New insights on obtaining phytoplankton concentration and composition from in situ multispectral Chlorophyll fluorescence, *Limnol. Oceanogr. Methods*, *8*, 695–708.
- Roesler, C. S., and A. H. Barnard (2013), Optical proxy for phytoplankton biomass in the absence of photophysiology: Rethinking the absorption line height, *Methods Oceanogr.*, *7*, 79–84.
- Roesler, C. S., et al. (2017), Recommendations for obtaining unbiased chlorophyll estimates from in situ chlorophyll fluorometers: A global analysis of WET Labs ECO sensors, *Limnol. Oceanogr. Methods*, doi:10.1002/lom3.10185.
- Sathyendranath, S., L. Lazzara, and L. Prieur (1987), Variations in the spectral values of specific absorption of phytoplankton, *Limnol. Oceanogr.*, *32*, 403–415.

- SATLANTIC (2013), *Operation manual for the OCR-504, SATLANTIC Operation Manual SAT-DN-00034, Rev. G*, 66 pp., Halifax, Nova Scotia, Canada.
- Schmechtig, C., H. Claustre, A. Poteau, and F. D'Ortenzio (2014), *Bio-Argo Quality Control Manual for the Chlorophyll-A Concentration*, Ifremer, France. [Available at <http://doi.org/10.13155/35385>.]
- Schmechtig, C., A. Poteau, H. Claustre, F. D'Ortenzio, G. Dall'Olmo, and E. Boss (2016), *Processing Bio-Argo Particle Backscattering at the DAC Level*, Ifremer, France. [Available at <https://doi.org/10.13155/39459>.]
- Siegel, D. A., S. Maritorena, N. B. Nelson, D. A. Hansell, and M. Lorenzi-Kayser (2002), Global distribution and dynamics of colored dissolved and detrital organic materials, *J. Geophys. Res.*, *107*(C12), 3228, doi:10.1029/2011JC000965.
- Sosik, H. M., and B. G. Mitchell (1995), Light absorption by phytoplankton, photosynthetic pigments and detritus in the California Current System, *Deep Sea Res., Part I*, *42*, 1717–1748.
- Sosik, H. M., and R. J. Olson (2002), Phytoplankton and iron limitation of photosynthetic efficiency in the Southern Ocean during late summer, *Deep Sea Res., Part I*, *49*, 1195–1216.
- Stedmon, C. A., and N. B. Nelson (2015), The optical properties of DOM in the ocean, in *Biogeochemistry of Marine Dissolved Organic Matter*, 2nd ed., edited by D. A. Hansell and C. A. Carlson, pp. 481–508, Academic, San Diego, Calif.
- Stramski, D., and D. A. Kiefer (1991), Light scattering by microorganisms in the open ocean, *Prog. Oceanogr.*, *28*, 343–383.
- Stramski, D., Bricaud, A., and A. Morel (2001), Modeling the inherent optical properties of the ocean based on the detailed composition of the planktonic community, *Appl. Opt.*, *40*, 2929–2945.
- Stramski, D., E. Boss, D. Bogucki, and K. J. Voss (2004), The role of seawater constituents in light backscattering in the ocean, *Prog. Oceanogr.*, *61*, 27–56.
- Suetin, V. S., V. V. Suslin, S. N. Korolev, and A. A. Kucheryavyi (2002), Analysis of variability of the optical properties of water in the Black Sea in summer 1998 according to the data of a SeaWiFS satellite instrument, *Phys. Oceanogr.*, *12*, 331–340, doi:10.1023/A:1021729229168.
- Sullivan, J. M., M. A. Twardowski, J. R. V. Zaneveld, and C. C. Moore (2013), Measuring optical backscattering in water, *Light Scatt. Rev.*, *7*, 189–224.
- Szeto, M., P. J. Werdell, T. S. Moore, and J. W. Campbell (2011), Are the world's oceans optically different?, *J. Geophys. Res.*, *116*, C00H04, doi:10.1029/2011JC007230.
- Tukey, J. W. (1958), Bias and confidence in no-quiet large samples, *Ann. Math. Stat.*, *29*, 614–623.
- Twardowski, M. S., E. Boss, J. B. Macdonald, W. S. Pegau, A. H. Barnard, and J. R. V. Zaneveld (2001), A model for estimating bulk refractive index from the optical backscattering ratio and the implications for understanding particle composition in case I and case II waters, *J. Geophys. Res.*, *106*, 14,129–14,142.
- Uitz, J., H. Claustre, F. B. Griffiths, J. Ras, N. Garcia, and V. Sandroni (2009), A phytoplankton class-specific primary production model applied to the Kerguelen Islands region (Southern Ocean), *Deep Sea Res., Part I*, *56*, 541–560.
- Valente, A., et al. (2016), A compilation of global bio-optical in situ data for ocean-colour satellite applications, *Earth Syst. Sci. Data*, *8*, 235–252, doi:10.5194/essd-8-235-2016.
- Vidussi, F., H. Claustre, B. Manca, A. Luchetta, and J.-C. Marty (2001), Phytoplankton pigment distribution in relation to the upper thermocline circulation in the Eastern Mediterranean Sea during winter, *J. Geophys. Res.*, *106*, 19,939–19,956.
- WETLabs (2016), *ECO Fluorometers and Scattering Sensors, User manual eco160114*, Edition B, 34 pp., Philomath, Ore.
- Wright, S. W., R. L. van den Enden, I. Pearce, A. T. Davidson, F. J. Scott, and K. J. Westwood (2010), Phytoplankton community structure and stocks in the Southern Ocean (30–80°E) determined by CHEMTAX analysis of HPLC pigment signatures, *Deep Sea Res., Part II*, *57*, 758–778.
- Xing, X., H. Claustre, S. Blain, F. D'Ortenzio, D. Antoine, J. Ras, and C. Guinet (2012), Quenching correction for in vivo chlorophyll fluorescence acquired by autonomous platforms: A case study with instrumented elephant seals in the Kerguelen region (Southern Ocean), *Limnol. Oceanogr. Methods*, *10*, 483–495.
- Xing, X., H. Claustre, J. Uitz, A. Mignot, A. Poteau, and H. Wang (2014b), Seasonal variations of bio-optical properties and their interrelationships observed by Bio-Argo floats in the subpolar North Atlantic, *J. Geophys. Res. Oceans*, *119*, 7372–7388, doi:10.1002/2014JC010189.
- Xing, X., H. Claustre, H. Wang, A. Poteau, and F. D'Ortenzio (2014a), Seasonal dynamics in colored dissolved organic matter in the Mediterranean Sea: Patterns and drivers, *Deep Sea Res., Part I*, *83*, 93–101.
- Xing, X., H. Claustre, E. Boss, C. Roesler, E. Organelli, A. Poteau, M. Barbieux, and F. D'Ortenzio (2017), Correction of profiles of in-situ chlorophyll fluorometry for the contribution of fluorescence originating from non-algal matter, *Limnol. Oceanogr. Methods*, *15*, 80–93, doi:10.1002/lom3.10144.
- Zaneveld, R., E. Boss, and A. Barnard (2001), Influence of surface waves on measured and modeled irradiance profiles, *Appl. Opt.*, *40*, 1442–1449, doi:10.1364/AO.40.001442.
- Zhang, X., L. Hu, and M. -X. He (2009), Scattering by pure seawater: Effect of salinity, *Opt. Express*, *17*, 5698–5710.
- Zibordi, G., F. Mélin, J.-F. Berthon, and E. Canuti (2013), Assessment of MERIS ocean color data products for European seas, *Ocean Sci.*, *9*, 521–533, doi:10.5194/os-9-521-2013.